BB

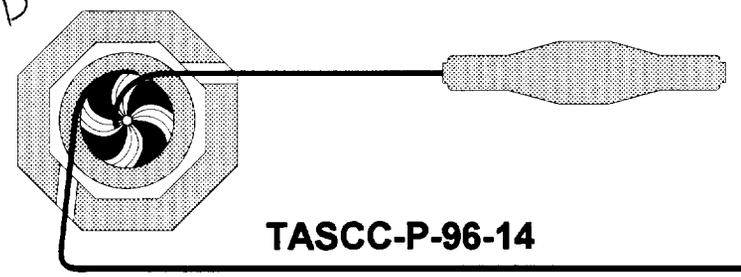

PREPRINT

tascc

TASCC-P-96-14

HIGH-SPIN STATES IN ODD-ODD ^{164}Lu

X.-H. Wang [a], C.-H. Yu [a, b, *], D.M. Cullen [a, †], D.C. Bryan [a], M. Devlin [a, ‡], M.J. Fitch [a], A. Galindo-Uribarri [c], R.W. Gray [a], D.M. Herrick [a], R.W. Ibbotson [a, §], K.L. Kurz [a], S. Mullins [d, ¶], S. Pilotte [e], D.C. Radford [c], M.R. Satteson [a], M.W. Simon [a], D. Ward [c], C.Y. Wu [a] and L.H. Yao [d]

[(a)] University of Rochester, NSRL, 271 E. River Road, Rochester, NY, 14627 USA
[(b)] Oak Ridge National Laboratory, Oak Ridge, TN, 37831-6371 USA
[(c)] AECL, Chalk River Laboratories, Chalk River, Ontario, K0J 1J0 Canada
[(d)] McMaster University, Hamilton, Ontario, L8S 4M1 Canada
[(e)] University of Ottawa, Ottawa, Ontario, K1N 6N5 Canada

* Current Address: Oak Ridge National Lab., Oak Ridge, TN, 37831-6371 USA
† Current Address: University of Liverpool, Oliver Lodge Lab., Liverpool, L69 3BX UK
‡ Current Address: Washington University, St. Louis, MO, 63130 USA
§ Current Address: Michigen State University, East Lancing, MI, 45824 USA
¶ Current Address: Australian National University, Canberra, ACT 0200, Australia

Submitted to
Nucl. Phys. A

Physical and Environmental Sciences
Chalk River Laboratories
Chalk River, ON K0J 1J0 Canada

1996 May

High-Spin States in Odd-Odd ^{164}Lu

X.-H. Wang[a], C.-H. Yu[a,b,*], D.M. Cullen[a,†], D.C. Bryan[a], M. Devlin[a‡] M.J. Fitch[a], A. Galindo-Uribarri[c], R.W. Gray[a], D.M. Herrick[a], R.W. Ibbotson[a§], K.L. Kurz[a], S. Mullins[d¶], S. Pilotte[e], D.C. Radford[c], M.R. Satteson[a], M.W. Simon[a], D. Ward[c], C.Y. Wu[a], L.H. Yao[d]

(a) University of Rochester, NSRL, 271 E. River Road, Rochester, NY 14627

(b) Oak Ridge National Laboratory, Oak Ridge, TN 37831-6371

(c) AECL, Chalk River Laboratories, Chalk River, K0J 1J0 Canada

(d) McMaster University, Hamilton, L8S 4M1 Canada

(e) University of Ottawa, Ottawa, K1N 6N5 Canada

Abstract

High-spin states in odd-odd ^{164}Lu have been studied using ^{19}F and ^{23}Na induced fusion-evaporation reactions. Three strongly-coupled rotational bands have been established and three decoupled bands were tentatively assigned to ^{164}Lu. The band crossing frequencies, energy signature splittings, and relative transition probabilities were deduced from experimental data and compared with neighboring even-even and odd-A nuclei. An anomalously large band crossing frequency was observed in the excited band, and a pronounced signature inversion was observed in the yrast band of ^{164}Lu. These anomalies may be associated with residual neutron-proton interactions.

NUCLEAR REACTIONS ^{149}Sm(^{19}F, 4n), E = 85 MeV; ^{146}Nd(^{23}Na, 5n), E = 110 MeV; measured E_γ, I_γ, $\gamma-\gamma$-coin. ^{164}Lu deduced levels, I, π, γ-branching, $B(M1)/B(E2)$ ratios, band crossings, signature inversion, neutron-proton interactions.

1. Introduction

Over the past two decades, studies of odd-odd nuclei at high angular momentum have been less extensive than studies of even-even and odd-A nuclei. This is mainly because an odd-odd nucleus has a higher level density and consequently experimental data are often much more complicated. In spite of this, odd-odd nuclei can offer rich information about nuclear structure, especially concerning the interplay between the single particle and collective motions. In particular, an odd-odd nucleus offers the unique possibility of probing the important but relatively

*Current address: Oak Ridge National Lab, Oak Ridge, TN 37831-6371.
†Current address: University of Liverpool, Oliver Lodge Lab, Liverpool, L69 3BX U.K.
‡Current address: Washington University, St. Louis, MO 63130.
§Current address: Michigen State University, East Lancing, MI 45824.
¶Current address: Australian National University, Canberra, ACT 0200, Australia.

unknown residual neutron-proton (n-p) interactions. Current state-of-the-art theoretical models often neglect neutron-proton interactions due to a lack of experimental data. To further our understanding of nuclear properties associated with odd-odd nuclei, we have studied high-spin states in ^{164}Lu, focusing on the following three experimental observables:

(1) Band crossings. Band crossing frequencies can be used to probe the strength of nuclear pair correlations, the relative positions of the proton and neutron Fermi levels, and the shape of the nucleus. For example, it is known[1, 2] that a band crossing occurs at a lower rotational frequency if the related pair correlation is smaller. This is the so called "blocking effect" that has been observed when comparing the neutron AB band crossing frequencies in even-even nuclei with those in their neighboring odd-N isotopes. The crossing frequencies are found to be systematically lower in odd-N nuclei than those in their even-even neighbors. This "blocking effect" has been attributed[1] to the reduced neutron pair correlations in an odd-N nucleus due to the presence of the odd neutron. In an odd-odd nucleus, the presence of both an odd neutron and an odd proton makes this "blocking effect" sensitive not only to neutron and proton pair correlations, but also to possible n-p interactions. Experimental phenomena related to this issue and their possible implications are discussed in subsection 3.1.

(2) Energy signature splittings. Signature splitting refers to the energy difference between the two signature sequences of one rotational band. Signature splitting can be related to nuclear structure information such as the single-particle configuration, the relative position of the Fermi level, and the deformation of the nucleus. For example, energy signature splittings in a number of odd-Z rare earth nuclei have been understood[4] as evidence for large negative-γ deformation. Signature dependence of quasiparticle energies in an odd-odd nucleus should provide information not only on the nuclear deformation, but also on the possible existence of n-p interactions. The signature splitting of rotational bands in ^{164}Lu is discussed in subsection 3.2.

(3) Transition rates. In a fast rotating nucleus, the B(E2) and B(M1) reduced transition probabilities reflect the collective- and single-particle aspects of the nuclear properties, respectively. These transition probabilities have been extensively studied in the neighboring odd-A nuclei. Therefore, a comparison of ^{164}Lu with its neighboring odd-A systems is very useful in searching for new properties associated with odd-odd nuclei.

High-spin states of ^{164}Lu were not studied prior to this work. However, a number of odd-odd

holmium and thulium nuclei have been studied[5, 6, 7, 8, 9, 10], and the neighboring odd-A isotopes and isotones of ^{164}Lu have been extensively studied[2, 3, 4, 11, 12, 13, 14, 16, 18]. These previous studies provide a good basis for the configuration assignments of bands in ^{164}Lu. They also facilitate a systematic analysis of properties of these nuclei. In the following, the experimental data and results will be presented in section 2, and the band crossings, energy signature dependence, as well as transition probabilities of ^{164}Lu will be discussed in comparison with its neighboring nuclei in section 3.

2. Experiments and results

2.1 EXPERIMENTS

Two experiments were carried out to populate high-spin states in ^{164}Lu. The first experiment was carried out at the Nuclear Structure Research Laboratory (NSRL) at the University of Rochester with the ^{149}Sm(^{19}F, 4n)^{164}Lu reaction. The 85-MeV ^{19}F beam was provided by the Rochester MP tandem accelerator and about 15 million γ-γ coincidence events were accumulated using the 8 Compton-suppressed Ge detectors of the NSRL. In this experiment, the 1 mg/cm^2, isotopically enriched ^{149}Sm target was backed by a thick Au foil (about 10 mg/cm^2) to stop the recoils. Doppler broadening effects were eliminated for all but the fastest transitions and the resolution was therefore optimized. The second experiment was performed at the TASCC facility of Chalk River Laboratories using the ^{146}Nd(^{23}Na, 5n)^{164}Lu reaction at a beam energy of 110 MeV. About 500 million double- or higher coincidence events were collected using the Chalk River 8π detector array[19], which consists of 20 Compton-suppressed Ge detectors and 71 BGO detectors operating as a total energy and multiplicity spectrometer. In this experiment, two isotopically enriched ^{146}Nd foils of about 500 $\mu g/cm^2$ each were stacked. Thin targets minimize the Doppler broadening of fast transitions from high-spin states. The analysis of data from both experiments established three strongly-coupled rotational bands in ^{164}Lu, and three decoupled bands were tentatively assigned to ^{164}Lu. A level scheme of these bands is shown in Fig. 1, and examples of gated spectra are shown in Fig. 2.

Since ^{164}Lu was not studied prior to this work, the assignments of bands in Fig. 1 to ^{164}Lu is mainly based on the multiplicity and sum-energy information obtained in the Chalk River experiment. In both experiments, the main contaminant reaction channels produce ^{164}Yb,

^{163}Yb, ^{165}Lu and ^{163}Lu. Fortunately, extensive high-spin data exist for these contaminant nuclei, see *e.g.* refs.[2, 11, 12, 13, 16], making it possible to identify gamma rays of ^{164}Lu by excluding known contaminants. The multiplicity and sum-energy information obtained from the 8π spectrometer proved to be very useful in identifying the reaction channels, especially for separating the 5n (channel of interest) from the 4n and 6n channels. Figure 3 shows a comparison of the multiplicity (or fold) and sum-energy spectra for the known transitions of ^{163}Lu (4n), ^{165}Lu (6n) and a transition assigned to ^{164}Lu (5n). In Fig. 3a, the channel number is equal to the experimental fold and in Fig. 3b, the channel number is directly proportional to the sum-energy.

For most of the transitions assigned to ^{164}Lu, their sum-energies and multiplicities have been checked against the main contaminants. It should be noted that the sum-energy and multiplicity of the p4n channel (producing ^{164}Yb) are virtually identical to those of the 5n channel (producing ^{164}Lu). However, since ^{164}Yb has been extensively studied[14, 15], misidentification of ^{164}Yb as ^{164}Lu is unlikely except for extremely weak decay sequences. For example, the yrast band of ^{164}Lu shown in Fig. 1 is clearly associated to either the 5n (^{164}Lu) or p4n (^{164}Yb) reaction channels according to the multiplicity and sum-energy spectra. A comparison of the intensities of the yrast band of ^{164}Lu with that of the yrast band of ^{164}Yb shows that the former is more intensely populated. If it belonged to ^{164}Yb, it should have been identified in previous studies. As a result, this band is assigned to ^{164}Lu with confidence. Band 2 and 3 are weaker than the yrast band. However, there is evidence that band 3 decays into the yrast band and band 2 of ^{164}Lu. Therefore, these two bands are also firmly assigned to ^{164}Lu. Bands 4, 5 and 6 are tentatively assigned to ^{164}Lu by comparing the associated multiplicity spectra. Due to their much weaker intensities and more severe contaminants, however, these assignments are not as certain as those for the other bands.

The ordering of the gamma rays in strongly-coupled rotational sequences is based on their coincidence relationships and energy-sums. The ordering of gamma rays in decoupled bands is based on their coincidence relationships as well as relative intensities.

The 20 detectors of the 8π array are arranged in four rings at polar angles of $\pm 37°$ and $\pm 79°$ with respect to the beam direction, and each ring has 5 detectors evenly distributed over the azimuthal angles. An angular correlation matrix was created by requiring coincidences of one gamma ray detected at $\pm 79°$ and the other detected at $\pm 37°$. Directional Correlations

of γ rays from Oriented states (DCO) were measured for strong transitions by computing the ratios of $T_\gamma(79)/T_\gamma(37)$ from the angular correlation matrix. Here $T_\gamma(79)$ is the gamma ray intensity measured in detectors located at $\pm 79°$ when it is in coincidence with another gamma ray detected at $\pm 37°$. $T_\gamma(37)$ is defined in a similar, but opposite way. These ratios were used to confirm the multipolarities of the gamma rays. The DCO ratios for most transitions in the three strongly-coupled bands are tabulated in Table 1. No reliable DCO ratios for bands 4, 5 and 6 could be deduced due to the lack of clean gates and weak intensities.

For the three strongly-coupled bands shown in Fig. 1, branching ratios defined as

$$\lambda = \frac{T_\gamma(I \rightarrow I-2)}{T_\gamma(I \rightarrow I-1)} \tag{1}$$

were extracted for most transitions. Here $T_\gamma(I \rightarrow I-2)$ and $T_\gamma(I \rightarrow I-1)$ are the γ-ray intensities of the $\Delta I = 2$ and $\Delta I = 1$ transitions, respectively. These intensities are measured in spectra gated above the transition of interest and corrected for efficiencies. The branching ratios were used to extract relative transition probabilities $B(M1, I \rightarrow I-1)/B(E2, I \rightarrow I-2)$ defined as:

$$\frac{B(M1, I \rightarrow I-1)}{B(E2, I \rightarrow I-2)} = 0.697 \frac{[E_\gamma(I \rightarrow I-2)]^5}{[E_\gamma(I \rightarrow I-1)]^3} \frac{1}{\lambda} \frac{1}{1+\delta^2} \tag{2}$$

Here δ is the $E2/M1$ mixing ratio for the $\Delta I = 1$ transitions, and $E_\gamma(I \rightarrow I-1)$ and $E_\gamma(I \rightarrow I-2)$ are the $\Delta I = 1$ and $\Delta I = 2$ transition energies, respectively. In the calculation, δ has been set to zero, since no mixing ratio could be deduced from the current data. The error associated with this assumption is expected to be small, since mixing ratios measured for the neighboring nuclei have been shown to be small (ref.[11]). The extracted $B(M1, I \rightarrow I-1)/B(E2, I \rightarrow I-2)$ ratios are shown in Fig. 4. These ratios are also tabulated in Table 1.

The relative intensities of γ rays were extracted and tabulated in Table 1. These intensities were corrected for efficiencies and normalized to the intensity of the 165.2-keV transition ($\equiv$ 500) in the yrast band. Note that the relative intensities are measured in the total projection or spectra gated on the bottom transition of the band. Such a restriction means that the errors associated with relative intensities are often larger than those associated with the branching ratios, since the latter were obtained by gating on clean transitions above each state of interest. It should also be noted that some transitions shown in the level scheme are weak or severely contaminated and their intensities are not listed.

2.2 LEVEL SCHEME AND CONFIGURATION ASSIGNMENTS

2.2.1 The Yrast Band. The configuration assignment of the yrast band in ^{164}Lu is mainly based on previous studies of its neighboring odd-odd and odd-A nuclei in mass 160 region. The proton $h_{11/2}$,$9/2^-[514]$ configuration is yrast in ^{163,165}Lu (refs.[11, 12, 13]), and low-K components of the $i_{13/2}$ neutron configurations are yrast in the odd-N nuclei in this mass region[2, 16]. As a result, the configuration of the yrast band for ^{164}Lu must be a low-K $i_{13/2}$ neutron coupled to an $h_{11/2}$,$9/2^-[514]$ proton. Since rotational bands associated with low-K $i_{13/2}$ neutrons have very large energy signature splittings, the lack of large signature splitting in the yrast band of ^{164}Lu (see Fig. 1) suggests that the $h_{11/2}$,$9/2^-[514]$ proton is the "signature-active" particle, *i.e.* this proton is mainly responsible for the B(M1) strength in the band.

The pattern of the aligned angular momentum of the yrast band also confirms the above assignment. The alignments of the six proposed bands of ^{164}Lu are shown in Fig. 5. This figure shows that the yrast band (open and closed squares) undergoes a band crossing at a rotational frequency of $\hbar\omega_c \approx 0.34$ MeV. This is consistent with the excitation of the second-lowest energy quasineutrons, the BC neutrons[‖]. BC neutron crossings have been observed at similar frequencies in the odd-A nuclei in this region (see, *e.g.* ref. [18]). The lowest-frequency neutron band crossing, the AB crossing, is absent in the yrast band, since the odd neutron already occupies the lowest-energy $i_{13/2}$ orbit, making the excitation of the AB quasineutrons impossible. At higher rotational frequency ($\hbar\omega \approx 0.5$ MeV), an upbend starts to occur in the $(-,0)$ signature. This is most likely the second-lowest proton crossing, the B_pC_p crossing (see table 2). The A_pB_p proton crossing is blocked in both signatures of the yrast band. However, the B_pC_p crossing is not blocked in the $(-,0)$ signature, since only the A_p proton [or the $(-,-1/2)$ proton] is occupied. This B_pC_p crossing is blocked in the $(-,1)$ signature, which is evident as the alignment of this signature sequence is flat at the highest spins. The $B(M1, I \to I-1)/B(E2, I \to I-2)$ ratios for the yrast band are also consistent with the above assignment, see more detailed discussions in subsection 3.3.

The spin assignment of this band is based on systematic trends of the yrast bands for odd-odd holmium[5] and thulium[8] isotopes, as well as the additivity of the alignments. Previous studies[5, 6, 8, 17] of odd-odd nuclei in this mass region have established a consistent pattern

[‖]See table 2 for the nomenclature of quasiparticle configurations used in this paper.

of the energy signature dependence. Therefore, it is most likely that ^{164}Lu follows that same trend. As a result, the signatures of the two sequences have been assigned so that the energy signature splitting of ^{164}Lu has the same phase as that of the neighboring odd-odd nuclei. To determine the spin of the lowest member of the rotational sequence, we considered the following two factors: (1) According to the Gallagher-Mozskowski rules[20], and an yrast configuration of $\pi 9/2^-[514] \otimes \nu 3/2^+[651]$, the most likely K-value for the yrast band is 6 $\hbar$. This means that the lowest transition of the rotational sequence should decay to a level with spin larger than or equal to 6 $\hbar$. In the case of the yrast band, the lowest member of the rotational sequence is the 258.2-keV transition. Thus the final level of the 258.2-keV transition should have a spin that is larger than or equal to 6 $\hbar$. (2) The initial alignment of the yrast band should be approximately equal to the sum of the initial alignments of the proton $9/2^-[514]$ and the neutron $i_{13/2}$ bands in the neighboring nuclei of ^{164}Lu. In order to evaluate this alignment additivity, the alignment of the yrast band of ^{164}Lu is compared with the neutron $i_{13/2}$ bands in ^{163}Yb and ^{165}Hf, as well as with the proton $9/2^-[514]$ bands in ^{163,165}Lu in Fig. 6. In this plot, the final level of the 258.2-keV transition of the yrast band of ^{164}Lu is assumed to have a spin of 10 $\hbar$. Figure 6 shows that the proton $9/2^-[514]$ bands in ^{163,165}Lu have an average initial alignment of about 1$\hbar$, and the neutron $i_{13/2}$ band in ^{163}Yb and ^{165}Hf have an average initial alignment of about 5 $\hbar$. The sum of these two initial alignments is almost exactly the initial alignment of 6$\hbar$ for the yrast band of ^{164}Lu. Such a comparison thus strongly supports the assignment of the 258.2-keV transition as $12^- \rightarrow 10^-$.

An additional check of the above spin assignment can be made with a comparison of the $12^- \rightarrow 10^-$ transition energies for the odd-odd N = 93 and N = 95 isotones shown in Fig. 7. This figure shows that the 258.2-keV transition of ^{164}Lu fits in with the systematic trend of the $12^- \rightarrow 10^-$ transitions for these odd-odd nuclei.

A few transitions at the bottom of the yrast band are firmly established to be in coincidence with the entire band but do not belong to the rotational sequence. The 101.0-, 184.3-, 171.7- and 161.5-keV transitions all decay out of the 10^- state, and they are not in mutual coincidence. The 142.2-keV transition is in coincidence with the 101.0-keV transition and the entire rotational band, but not in coincidence with the 184.3-, 171.7- and 161.5-keV transitions. The DCO ratios for these transitions are difficult to measure due to their low intensities. For those transitions for which DCO ratios can be determined, their multipolarities are still difficult to determine.

This is because at low spins the nuclear orientation alignment is sufficiently attenuated[21], and since the band decays to low spins through a mixture of dipole and quadrupole transitions, the differences between the DCO ratios of transitions with different multipolarities are smaller at very low spins. As a result, the final states of these non-rotational transitions at the bottom of the yrast band have not been assigned spins and parities.

2.2.2 Band 3. Band 3 consists of strongly coupled sequences and feeds into the yrast band as well as band 2. The intensity of band 3 is only about one tenth and one third of the yrast band and band 2, respectively. Tentative connecting transitions from band 3 to the yrast band and band 2 are shown as dotted lines in Fig 1. In Fig. 2(c) the spectrum obtained by gating on the 222.0-keV transition in this band shows both the 864.7-keV, 964.7-keV transitions connecting to the yrast band, and the 648.3-keV transition connecting to band 2. The low-spin transitions of the yrast band (indicated by down triangles) and those in band 2 (indicated by diamonds) are also shown to be in coincidence with band 3. Although the three connecting transitions are weak, tentative DCO ratios can be extracted and the ratios for the 964.7- and 864.7-keV transitions connecting to the yrast band suggest that they are dipole transitions. Due to their relatively large energies, they are most likely E1 transitions instead of M1 transitions. The spin and parity assignments of band 3 are, therefore, mainly based on the multipolarity of these two connecting transitions.

The alignment of band 3 has a rather large average value below the band crossing that starts at $\hbar\omega_c \approx 0.38$ MeV, see Fig. 5. Such a large initial alignment strongly suggests that this is a four-quasiparticle band. The most likely four-quasiparticle configuration in an odd-odd nucleus is for the odd proton and the odd neutron to couple to a pair of excited quasiparticles. The obvious candidate for the pair of excited quasiparticles is the lowest-energy $i_{13/2}$ neutrons, since this is the quasiparticle pair that is excited at the lowest frequency in this mass region. The odd neutron could occupy the $3/2^-[521]$, the $5/2^-[523]$ or the $11/2^-[505]$ state, see Nilsson diagrams for neutrons in Fig. 8. The very large B(M1)/B(E2) ratios of this band (see Fig. 4) suggest that the $11/2^-[505]$ neutron state is most favored, since it has a large K-value and a large negative g-factor (which enhances the total B(M1) value when coupled to the proton). If we take the parity of band 3 to be positive (determined by the proposed E1 connecting transitions to the yrast band), then since the odd neutron has negative parity, the parity of the odd proton must also be negative. The only negative-parity orbits in the vicinity of the

proton Fermi level of ^{164}Lu that could have strong M1 transitions are the high-K $h_{11/2}$ protons, among which the $9/2^-[514]$ configuration is the lowest in energy. As a result, the configuration of band 3 is assigned as $\pi 9/2^-[514] \otimes \nu 11/2^-[505] \otimes [\nu i_{13/2} \times 2]$.

The band crossing occurring at $\hbar\omega_c \approx$ 0.38 MeV in band 3 probably corresponds to the excitation of the lowest-energy negative-parity neutron pair, or the EF crossing (see table 2). According to Cranked Shell Model (CSM) calculations for ^{164}Lu, the EF crossing normally occurs at a frequency beyond 0.45 MeV for a quadrupole deformation of $\beta_2 = 0.21$. However, according to these calculations, the EF crossing frequency decreases with decreasing deformation. At a quadrupole deformation of $\beta_2 = 0.15$, the EF crossing frequency is reduced to $\hbar\omega_c \approx 0.38$ MeV. The occupation of the $9/2^-[514]$ proton and the $11/2^-[505]$ neutron could result in a relatively small quadrupole deformation, since both orbits are strongly up-sloping in the Nilsson diagram (see Fig. 8) and can drive the nucleus towards a much smaller deformation. Therefore, it is possible that the observed crossing in band 3 is the EF neutron crossing.

2.2.3 Band 2. Band 2 is the second strongest band populated in ^{164}Lu. The decay of this band to the yrast band has not been established, possibly due to very weak connecting transitions or isomeric states at the band head.

The parity of band 2 is most likely even, based on the 648.3-keV transition that connects band 3 to band 2. The DCO ratio for the 648.3-keV transition is 1.02 (0.21), suggesting that it is most likely an E2 transition. The parity and spins of band 2 are, therefore, assigned based on this connecting transition.

It should be noted that even though the connecting 648.3-keV, 864.7-keV and 964.7-keV transitions are weak and only tentatively placed in the level scheme, the resulting spin assignments for band 2 and band 3 produce a relative energy pattern for the three strongly-coupled bands that is consistent with the observed relative intensities. For example, the experimental routhians shown in Fig. 9 confirm that the assigned spins result in the expected trend of increasing excitation energies with decreasing intensities (see also table 1 for relative intensities).

The band crossing observed in band 2 occurs at a rotational frequency of $\hbar\omega_c \approx 0.28$ MeV, see Fig. 5. Since this is the lowest-frequency band crossing observed in ^{164}Lu, and the AB neutron crossing occurs at the the lowest frequency for nuclei in this mass region, this crossing is identified as the AB neutron crossing, *i.e.* it is caused by the excitation of the lowest-energy $i_{13/2}$ quasineutrons. The odd neutron involved in band 2, therefore, must not be related to the

$i_{13/2}$ configuration, but can be either the $5/2^-[523]$ or the $3/2^-$ [521] state, see Fig. 8. The systematic trend of band head energies show, however, that the $5/2^-$ [523] state may have a lower excitation energy in ^{164}Lu than the $3/2^-[521]$ state. For the proton, the only possible configuration is the $9/2^-[514]$ state, because of the positive parity of band 2. Therefore, we tentatively assign band 2 as the $\pi 9/2^-[514] \otimes \nu 5/2^-[523]$ configuration.

It is worth noting that when alignment additivity is considered for band 2 in a manner similar to that described in subsection 2.2.1, the result is not satisfactory. On the other hand, no other possible configuration can produce a satisfactory alignment additivity except for the $\pi 7/2^-[404] \otimes \nu i_{13/2}$ configuration. If this is the configuration for band 2, then the crossing occurring at $\hbar\omega_c \approx 0.28$ MeV has to be a BC neutron crossing. However, BC crossing frequency is already established in the yrast band to be $\hbar\omega_c \approx 0.34$ MeV, and there's no reason that the BC crossing should occur at a much lower frequency in band 2 than in the yrast band. As a result, the $\pi 7/2^-[404] \otimes \nu i_{13/2}$ configuration is unlikely and from other considerations described in previous paragraphs, the $\pi 9/2^-[514] \otimes \nu 5/2^-[523]$ configuration is still the most likely configuration for band 2.

2.2.4 Band 4, 5 and 6. Band 4, 5 and 6 are decoupled (only one signature sequence is observed), and thus both proton and neutron origins must have large signature splittings. For the neutrons, this could be the $3/2^+[651]$, $5/2^-[523]$ or $3/2^-[521]$ configurations, with the $i_{13/2}$, $3/2^+[651]$ orbit having the lowest energy (see Fig. 8); For the protons, the possible orbits are the $1/2^-[541]$ and the $3/2^+[411]$ orbits, with the $1/2^-[541]$ orbit being much more favored at high spin (see Fig. 8). In Fig. 5, all the three decoupled bands (band 4, 5 and 6) show an upbend at $\hbar\omega_c \approx 0.32$ — 0.35 MeV, where the BC neutron crossing is observed in the yrast band. However, it is difficult to determine whether the upbend in any of these three decoupled bands is caused by the same BC crossing or is a delayed AB crossing. The latter is possible if the proton $1/2^-[541]$ orbit is involved. From previous studies[11, 12, 13] of ^{163,165}Lu, it has been observed that the $h_{11/2}$,$1/2^-[541]$ band has a delayed AB neutron band crossing due to the larger quadrupole deformation associated with this band. Since there are many uncertainties involved, the present experiment cannot provide any firm assignment of configurations to these three bands. The spins given in Fig. 1 are simply best guesses.

It should be pointed out that the proton configurations for these three decoupled bands are unlikely to involve the proton $1/2^+[660]$ configuration, even though this band has been

observed[11, 13] in ^{163,165}Lu. This is mainly because the $1/2^+[660]$ orbit has a strong shape polarization effect (see Fig. 8) and bands associated with this orbit are expected to have a larger quadrupole deformation than other bands. In the absence of lifetime measurements, the magnitude of $J^{(2)}$ moment of inertia can be used to qualitatively estimate the relative magnitude of quadrupole deformations, and these are illustrated in Fig. 10 for ^{163}Lu and ^{164}Lu. In Fig. 10(a), the $J^{(2)}$ moment of inertia for the $9/2^-[514]$, $7/2^+[404]$, and the $1/2^-[541]$ bands of ^{163}Lu all have an average value of $30 - 50\ \hbar^2/MeV$ (excluding the band crossing regions where the $J^{(2)}$ peaks at much higher values). The only band that has a significantly larger average $J^{(2)}$ values ($J^{(2)} = 50 - 70\ \hbar^2/MeV$) is the $1/2^+[660]$ band, see the open diamonds. For ^{164}Lu, all bands shown have a similar $J^{(2)}$ of $30 - 55\ \hbar^2/MeV$. None of the three decoupled bands in ^{164}Lu (band 4, 5 and 6 denoted by open triangles, closed triangles, and open circles, respectively in Fig. 9(b)) shows any significantly larger $J^{(2)}$ values relative to the yrast band. Therefore it is unlikely that any of these three decoupled bands contain the proton $1/2^+[660]$ configuration.

3. Discussion

3.1 AB NEUTRON BAND CROSSING SYSTEMATICS

Three neutron band crossings are observed in ^{164}Lu: The AB neutron band crossing in band 2, the BC crossing in the yrast band, and the EF crossing in band 3 (see Fig. 5). Band crossing frequencies are determined by a number of parameters related to the structure of the nucleus, among which are: (1) The nuclear pair correlations; (2) The position of the Fermi level relative to the orbits responsible for the crossing; (3) The deformation of the nucleus. As a result, band crossing frequencies can be used as an indirect measure of these properties. Since such a measure is indirect, only relative information can provide meaningful indications. In the following, we will compare the AB neutron band crossing frequencies observed in ^{164}Lu with those in neighboring nuclei.

Figure 11 summarizes the AB neutron crossing frequencies ($\hbar\omega_c$) observed in the yrast bands of the even-even Yb isotopes (open circles), those in the negative-parity bands of the odd-N Yb isotopes (closed circles) and those in the odd-odd ^{164}Lu and ^{160,164}Tm nuclei (stars). The crossing frequencies in the odd-N Yb isotopes are systematically reduced relative to those in the yrast bands of even-even isotopes due to the so called "blocking effect" of the odd neutron[1, 2].

The odd neutron reduces the neutron pair correlations in an odd-N nucleus. Therefore, it does not need to rotate as fast as an even-even nucleus in order for the Coriolis plus centrifugal forces to compensate for the effects of neutron pair correlations. As a result the neutron band crossing occurs at a lower rotational frequency in an odd-N nucleus than in an even-even nucleus. For an odd-odd nucleus, the simplest approximation would assume that it has the same neutron pair correlation as an odd-N, even-Z nucleus. Therefore, similar "blocking" effects should occur, *i.e.* the neutron band crossing frequencies in odd-odd nuclei should be reduced relative to their neighboring even-even nuclei. This is indeed observed[27] in odd-odd ^{164}Tm, which has an $\hbar\omega_c \approx$ 0.23 MeV, similar to the average $\hbar\omega_c$ observed in the odd-N Yb isotopes (Fig. 11). The striking feature shown in Fig. 11, however, is the disappearance of this blocking effect in the odd-odd nuclei ^{164}Lu and ^{160}Tm (ref.[6]). The crossing frequencies in these two odd-odd nuclei are the same as those in the even-even Yb isotopes. Such a phenomenon is difficult to understand in terms of the standard CSM theory that associates the neutron band crossing frequency to the neutron pair correlations and assumes no correlations between the odd proton and the odd neutron.

In order to exclude other effects that may affect the neutron band crossing frequency, we have estimated the influence of quadrupole deformation (β_2) on the AB neutron crossing in this mass region. Figure 12 shows the Cranked Shell Model (CSM) calculations of the β_2 dependence of the AB neutron band crossing frequency for nuclei in this mass region. The Total Routhian Surface (TRS) calculations predict that these nuclei have negligible differences in γ- and β_4 deformations. Therefore, calculations were performed at fixed values of γ and β_4. Also indicated in Fig. 12 are the β_2 values predicted by the TRS calculations for ^{164}Lu, ^{160}Tm, ^{164}Tm and two examples of the odd-N Yb isotopes, ^{163}Yb and ^{165}Yb. These calculations indicate that: (1) Assuming the same neutron pair correlation for odd-odd and odd-N, even-Z nuclei, the influence of β_2 deformation on $\hbar\omega_c$ is small; (2) Taking into account this small influence, ^{164}Lu and ^{160}Tm should have a smaller AB band crossing frequency than ^{164}Tm or their neighboring odd-N Yb isotopes due to their smaller quadrupole deformation. Therefore, if deformation has any influence on band crossing frequency at all for these nuclei, it is expected to result in the opposite of what is observed in experiments, see Fig. 11. Consequently, deformation differences cannot explain the larger-than-expected $\hbar\omega_c$'s observed in ^{164}Lu and ^{160}Tm.

An alternative explanation for the anomalously large AB neutron crossing observed in ^{164}Lu

and ^{160}Tm is that neutron-proton interactions become important in these two nuclei due to their odd-odd nature, and that these interactions have a significant influence on band crossings. Therefore a simple CSM calculation without the inclusion of proper neutron-proton interactions cannot reproduce the observed phenomenon.

It should be noted that the above anomalous band crossings do not always occur in odd-odd nuclei. As shown in Fig. 11, ^{164}Tm has a "normal" AB neutron crossing. The fact that ^{160}Tm and ^{164}Lu show the anomalous band crossing and ^{164}Tm does not, seems to indicate that neutron-proton interactions are sensitive to specific single-particle configurations.

It is also interesting to note that the alignment gains associated with the AB band crossing are different for even-even nuclei, even-Z, odd-N nuclei, and odd-odd nuclei. The average alignment gain associated with the AB neutron band crossing is about $10\hbar$ for even-even nuclei, and $7.5\hbar$ for even-N, odd-Z nuclei. For odd-odd ^{164}Lu and ^{160}Tm, the alignment gains are 6.8 and $5\hbar$, respectively. It is unclear why the alignment gain for the odd-odd nuclei is about 40% smaller than the even-even nuclei and about 25% smaller than the odd-N, even-Z nuclei. A previous study[28] on ^{186}Au also observed reduced alignment gains in odd-odd nuclei and attributed this reduction to residual n-p interactions.

3.2 ENERGY SIGNATURE SPLITTINGS

The signature dependence of a rotational band is related to the K quantum number of the associated single-particle state, and to the deformation of the nucleus. In the three strongly-coupled bands of ^{164}Lu, the energy signature splitting is small compared with that of its neighboring odd-Z, even-N nuclei. In order to illustrate this small signature splitting, an energy difference, ΔE, defined as

$$\Delta E(I) = [E(I) - E(I-1)] - [E(I+1) - E(I) + E(I-1) - E(I-2)]/2 \qquad (3)$$

is plotted as a function of spin for the three bands of ^{164}Lu together with the yrast bands of ^{163,165}Lu in Fig. 13. Here $E(I)$ is the level energy of state I. It is apparent that $\Delta E(I)$ is directly proportional to the real energy signature splitting

$$\delta E(I) = E(I) - [E(I+1) + E(I-1)]/2 \qquad (4)$$

but magnified by approximately a factor of two.

In Figs. 13(a), (b) and (c), the energy signature splitting ΔE of the three strongly-coupled bands in ^{164}Lu are plotted and compared with those of the $\pi h_{11/2}, 9/2^-[514]$ bands of ^{163,165}Lu shown in Figs. 13(d) and 13(e). In Figs. 13(d) and (e), the $\alpha = 1/2$ signature (the sequence with spins, I = 1/2, 5/2, ...) and the $\alpha = -1/2$ signature (the sequence with spins, I = 3/2, 7/2, ...) are denoted by closed and open symbols, respectively. These two figures show that the $\alpha = -1/2$ signature is favored at low angular momentum (below the AB neutron crossing) for ^{163,165}Lu. This has been interpreted[3, 11, 29] as evidence of a sizable negative-γ deformation in these nuclei at low spin. The yrast band of ^{164}Lu is most likely the result of the $\alpha = 1/2$ signature of the $i_{13/2}$,$3/2^+[651]$ neutron coupled to the two signatures of the $h_{11/2}$,$9/2^-[514]$ proton. Therefore, the $\alpha = 0$ signature of ^{164}Lu yrast band (result of the favored $\alpha = -1/2$ signature of the $9/2^-[514]$ proton coupled to the favored $\alpha = 1/2$ signature of the $i_{13/2}$ neutron) is expected to be energetically favored. However, Fig. 13(a) shows that at low spin the $\alpha = 0$ signature (open circles) of ^{164}Lu is unfavored. This phenomenon has been previously observed in other odd-odd nuclei (see, *e.g.* refs.[8, 9, 10]), and has been referred to as the "signature inversion". Fig. 13(a) also shows that the energy signature dependence of ^{164}Lu changes phase at a spin of $I \approx 18\hbar$ and becomes normal. This phase change corresponds to the onset of the BC neutron band crossing, see Figs. 1 and 5.

Signature inversion has never been observed in one-quasiproton bands. It has, however, been observed in three-quasiparticle bands of odd-Z, even-N nuclei in the rare earth region. For example, in ^{163,165}Lu, the energy signature splitting is slightly inverted above the AB neutron band crossing in the yrast bands (see Figs. 13(d) and (e)). This has been interpreted[30] as the result of a positive-γ deformation induced by the shape-driving effect of the $i_{13/2}$ neutrons which are excited at the band crossing. Similar interpretations have also been given[31] to explain the signature inversion observed at low spin in odd-odd nuclei. However, self-consistent calculations of Total Routhian Surfaces (TRS) predict a very small γ deformation for ^{164}Lu. For the yrast band at low spin, the predicted γ deformation for ^{164}Lu is $-2.1°$. While this does not support the interpretation of a large positive-γ deformation being responsible for the observed signature inversion, the extracted γ deformation from the TRS may not be accurate since no n-p interaction is included in the calculation.

It is interesting to note that for ^{163}Lu and ^{165}Lu, a small signature inversion is induced at the AB neutron crossing. This seems to support the argument that positive-γ deformation is

responsible for the observed signature inversion. Both the s-band (portion of the yrast band above AB neutron crossing) of the ^{163,165}Lu and the ground band of ^{164}Lu involve $i_{13/2}$ neutrons, and they both have inverted signature splittings. Thus, the positive-γ shape driving force of $i_{13/2}$ neutrons may be responsible. However, this does not explain why the signature inversion disappears at the onset of BC crossing for ^{164}Lu, since the excitation of the second pair of $i_{13/2}$ neutrons (BC neutrons) should have a similar shape driving force as the AB neutrons. Thus if positive-γ is the only cause for such a signature inversion, it should remain throughout the yrast band of ^{164}Lu. Both the predicted small, negative-γ deformation and the unexplained disappearance of the inversion at BC crossing for ^{164}Lu suggest that positive-γ deformation cannot be the only cause for the observed signature inversion.

In an article[32] discussing signature inversion in odd-odd ^{156}Tb and ^{160}Ho, Hamamoto pointed out that signature inversion can occur in axially symmetric odd-odd nuclei at spins $I \leq j_p + j_n$ for certain shell fillings of particles. However, in the case of the yrast band in ^{164}Lu, $j_p + j_n = \frac{11}{2} + \frac{13}{2} = 12\ \hbar$, whereas signature inversion was observed up to spin 18 $\hbar$. Thus particular shell fillings of the particles may not satisfactorily explain the signature inversion in ^{164}Lu.

An alternative interpretation of such signature inversion is that it is caused by residual neutron-proton interactions. Such interactions may be enhanced in an odd-odd nucleus due to the presence of an unpaired proton and an unpaired neutron. It has been suggested[33, 34] that calculations with the inclusion of proper n-p interactions can reproduce the experimental signature inversion in an odd-odd nucleus. It is unclear, however, what is the correlation of the n-p interactions and the disappearance of the inversion at spin $18\hbar$ in the yrast band.

The signature splitting for band 2 of ^{164}Lu shows no signature inversion, see Fig. 13(b). The phase of the signature splitting of band 2 is normal and the AB band crossing has no influence on this signature dependence. It is interesting to compare the signature splitting of band 2 to the $\pi 9/2^-[514]$ bands of ^{163,165}Lu shown in Figs. 13(d) and (e), and note that the large signature splitting in the proton $9/2^-[514]$ band is significantly quenched in band 2 of ^{164}Lu due to the coupling of the neutron $5/2^-[523]$ state.

For band 3, signature splitting is small throughout the band. However, the phase of the splitting changes at spin $I \approx 26$, where the proposed EF neutron crossing starts to occur. This signature inversion is again difficult to understand in terms of nuclear shape changes, since EF

neutrons are not expected to have any significant shape-driving forces.

The cause of signature inversion is not completely understood. However, experimental evidence seems to indicate that such a phenomenon is sensitive to quasiparticle configurations as well as possible n-p interactions. More experimental data and further theoretical investigations are needed in order to fully understand this phenomenon.

3.3 TRANSITION PROBABILITIES

The ratio of the reduced transition probabilities of the stretched electric quadrupole [B(E2)] and magnetic dipole [B(M1)] transitions for the three strongly-coupled bands in ^{164}Lu are deduced from experimental branching ratios according to Eq. 2. and plotted as a function of rotational frequency in Fig. 4. The branching ratios and the $B(M1, I \rightarrow I-1)/B(E2, I \rightarrow I-2)$ ratios for these three bands are also tabulated in Table 1. The B(M1)/B(E2) ratios for the three bands are compared with calculated values which are shown as solid curves. These calculations are carried out using a geometric formula[35] for B(M1) values extended[28] for odd-odd nuclei:

$$B(M1, I \rightarrow I-1) = \frac{3}{8\pi}\frac{1}{I^2}\left[(g_p - g_R)(k_p\sqrt{I^2-K^2} - i_pK) - (g_n - g_R)i_nK - (g_a - g_R)i_aK\right]^2 \mu_N^2 \quad (5)$$

Here g_p, g_n, k_p, i_p, i_n are the g factors, K values, and aligned angular momentum for the odd proton (those with subscript p) and odd neutron (those with subscript n), respectively. g_R is the g factor of the core and K represents the K value of the band in the odd-odd nucleus. The terms g_a and i_a represent the g factor and aligned angular momentum of the particle configuration aligned at the band crossing. The g factors used for the above calculations were chosen based on previous studies of nuclei in the same mass region with the assigned configurations in ^{164}Lu. The alignments of various configurations are extracted from experimental data. These parameters are summarized in Table 3. In order to compare the calculation with experimental data, the B(E2) values were calculated according to the following equation:

$$B(E2, I \rightarrow I-2) = \frac{5}{16\pi} < IK20|I-2K >^2 Q_0^2 \quad (6)$$

Here Q_0 was chosen to be 5.8 *eb* for the yrast band and band 2, and for band 3, $Q_0 = 5.0$ *eb* was chosen to take into account the strongly upsloping neutron and proton high-K $h_{11/2}$ orbits occupied by the odd neutron and odd proton (see Fig. 8 and discussions in subsection

2.2.3). In calculations for the yrast band and band 2, the core g factor, g_R, was decreased by approximately 25% for transitions above the band crossing to take into account the change of moment of inertia due to the reduced neutron pair correlations. More detailed discussions of the transition rates for the three bands are presented in the following three subsections.

3.3.1 The yrast band. At low angular momentum the B(M1)/B(E2) ratios for the yrast band decrease with spin and the trend is well reproduced by the the calculation, see Fig. 4. Below the BC crossing, the average value of the ratios is about 1.25 μ_N^2/e^2b^2. This is a factor of two more than the average ratio for the low spin portion of the $\pi 9/2^-[514]$ band in ^{163}Lu (ref.[11]). Such an increased B(M1)/B(E2) ratio in ^{164}Lu can be understood as the result of the increased B(M1) values due to the contribution of the $i_{13/2}$ neutron, which has a negative g-factor. At the point where the BC band crossing occurs ($\hbar\omega_c \approx 0.34$ MeV), the $B(M1, I \rightarrow I-1)/B(E2, I \rightarrow I-2)$ ratios begin to rise as a function of spin. This increase can be partially attributed to the increase of $B(M1)$ values due to the BC crossing. The magnetic transition probability is most sensitive to the change of single particle configurations. The excitation of the BC quasineutrons, which have a negative g factor, is thus expected to increase the B(M1) values. This is also predicted by the calculation as shown by the solid curve. Above the crossing, the experimental B(M1)/B(E2) ratios continue to rise, whereas the calculation predicts a smooth decrease of the ratio with increasing frequency. It is not clear what may cause the experimental B(M1)/B(E2) ratios to rise at this point, since no obvious band crossings are observed. It is possible that this increase is the result of a decreasing B(E2) values, which is not considered in the calculation. The present data, however, are not sufficient for the extraction of absolute B(M1) and B(E2) values, thus it is difficult to determine the exact cause of this rise at high spin.

3.3.2 Band 2. The average experimental $B(M1, I \rightarrow I-1)/B(E2, I \rightarrow I-2)$ ratios below the AB neutron crossing for band 2 is approximately 0.45 μ_N^2/e^2b^2. This is only about one third of that of the yrast band. The primary reason for the smaller ratios of band 2 compared with those of the yrast band is the different g factor of the odd neutron. In the yrast band, the B(M1) rates of the signature-active odd proton are enhanced when the proton is coupled to an $i_{13/2}$ neutron, which has a negative g factor (see Eq. 5). The relatively large initial alignment of the $i_{13/2}$ neutron (approximately 5 $\hbar$) also contributes to the enhanced B(M1) rates. For band 2, the situation is the opposite: The B(M1) strength of the signature-active

proton is reduced when the proton is coupled to the $5/2^-[523]$ neutron, which has a positive g factor, and the initial alignment of the neutron configurations is very small (about 0.5 $\hbar$). These ratios increase by a factor of two at the AB neutron band crossing at $\hbar\omega_c \approx 0.28$ MeV, and decrease with $\hbar\omega$ above the crossing. The general trend of the frequency dependence of the $B(M1, I \rightarrow I-1)/B(E2, I \rightarrow I-2)$ ratios is predicted by the theoretical calculation (see the solid curve in Fig. 4). However, the calculation overpredicts the ratios by approximately 40% below the band crossing and 20% above the crossing. The discrepancy between the calculated and measured B(M1)/B(E2) ratios could be caused by a number of reasons, one of which may be the inaccurate parameters used in the calculation.

We also examined the possibility of different neutron and proton configurations for band 2 in order to see whether other configuration assignments would produce a better agreement between the calculation and experiment. The comparison shows that no other possible configuration can reduce this discrepancy. For example, a change of the proton configuration from the $9/2^-[514]$ to the $7/2^+[404]$ state results in a curve that is a factor of three smaller than the experimental data. As a result, the proton $7/2^+[404]$ configuration is ruled out. A change of the neutron configuration from the $5/2^-[523]$ to $3/2^-[521]$ state only changes the calculated result by less than 10%, and thus it is difficult to distinguish these two neutron configurations in terms of B(M1) values.

3.3.3 Band 3 The $B(M1, I \rightarrow I-1)/B(E2, I \rightarrow I-2)$ ratios for band 3 are the largest among the three strongly coupled bands. The average value of the ratios is approximately 1.5 $(\mu_N/eb)^2$. These large B(M1)/B(E2) ratios strongly suggest that the band involves more than two quasiparticles. The tentative spin assignment for this band also results in an alignment that is consistent with a band that has the AB neutrons excited. As discussed in subsection 2.2.3, the most likely configuration for this band is $\pi 9/2^-[514] \otimes \nu 11/2^-[505] \otimes [\nu i_{13/2} \times 2]$. With a constant Q_0 of 5.0 eb, and parameters consistent with the above configuration, the calculation qualitatively reproduces the experimental ratios except for the two highest-spin states. At high spin, the calculation predicts a decrease of B(M1)/B(E2), whereas the experimental ratios stay constant. It should be noted that the last two data points for band 3 also correspond to the beginning of the suggested EF neutron band crossing (compare Figs. 4 and 5), which could enhance the B(M1) values, and the calculation has not taken this crossing into account. The larger experimental B(M1)/B(E2) ratios at the highest spins may also be caused by decreased

B(E2) values.

It should be pointed out that the above calculations are based on a simplified model with approximations such as a constant Q_0. To further understand the information carried by these transition probabilities, lifetimes of these transitions must be measured in order to extract absolute B(M1) and B(E2) probabilities. In addition, theoretical calculations also need to take into account important parameters such as the n-p interactions, and more accurate g factors are needed in order to improve the quality of the calculation.

4. Summary

High-spin states of ^{164}Lu were populated using the ^{19}F and ^{23}Na induced fusion-evaporation reactions. Three strongly coupled rotational bands were assigned to ^{164}Lu, and three decoupled bands tentatively assigned. A comparison of the AB neutron band crossing frequency observed in ^{164}Lu with its even-even and odd-N ytterbium isotopes shows that the crossing frequency is anomalously higher than expected. A neighboring odd-odd nucleus, ^{160}Tm, shows a similar anomaly, whereas ^{164}Tm has a "normal" crossing frequency. Deformation differences cannot explain this anomaly. One possible explanation is that it is caused by residual neutron-proton interactions. Energy signature splittings of the three strongly coupled bands in ^{164}Lu are compared with neighboring ^{163,165}Lu isotopes. The yrast band of ^{164}Lu shows a pronounced signature inversion which cannot be attributed to a γ deformation effect. Such a inverted energy signature splitting may also be partially attributed to residual n-p interactions. It is interesting to note that signature inversion only occurs in the yrast band of ^{164}Lu, and not in the two excited bands. Relative transition probabilities, $B(M1, I \rightarrow I-1)/B(E2, I \rightarrow I-2)$ ratios, are extracted for the three strongly-coupled bands in ^{164}Lu and are compared to calculations based on a geometric model and assuming a constant Q_0. The $B(M1, I \rightarrow I-1)/B(E2, I \rightarrow I-2)$ ratios for the yrast band are well reproduced for $\hbar\omega < 0.4$ MeV, above which the experimental ratios increase with $\hbar\omega$, the cause of which is not fully understood. The theoretical calculations of $B(M1, I \rightarrow I-1)/B(E2, I \rightarrow I-2)$ for band 2 overpredict the data by 20 - 40%, whereas calculations for band 3 reasonably reproduce the data. The anomalies exhibited in the experimental results of ^{164}Lu calls for further theoretical investigations, especially regarding the issue of neutron-proton interactions.

Acknowledgements

Research at the Nuclear Structure Research Laboratory of the University of Rochester is supported by the National Science Foundation. Oak Ridge National Laboratory is managed by Lockheed Martin Energy Research Corporation for the U.S. Department of Energy under contract number DE-AC05-96OR22464.

Note: At the time when this article is being sent for publication, we are aware of two publications that have just appeared in journals reporting studies of ^{164}Lu: (1) P. Juneja, *et al.*, Phys. Rev. **C53** (1996) 1221; (2) M.A. Cardona, *et al.*, Z. Phys. **A354** (1996) 5. Juneja *et al.* reported four rotational bands in ^{164}Lu, three of which overlap with the yrast band, band 2 and band 5 presented in this article. For the yrast band and band 2, our work established the rotational sequences to substantially higher spins than those reported by Juneja *et al.* Cardona *et al.* only reported the yrast band of ^{164}Lu up to spin $29^{-}\hbar$.

References

[1] J.D. Garrett, G.B. Hagemann and B. Herskind, Ann. Rev. Nucl. Part. Sci. **36** (1986) 419

[2] J. Kownacki, J.D. Garrett, J.J. Gaardhøje, G.B. Hagemann, B. Herskind, S. Jósson, N. Roy, H. Ryde, and W. Waluś, Nucl. Phys. **A394** (1983) 269

[3] C.-H. Yu, M.A. Riley, J.D. Garrett, G.B. Hagemann, J. Simpson, P.D. Forsyth, A.R. Mokhtar, J.D. Morrison, B.M. Nyakó, J.F. Shapey-Schafer and R. Wyss, Nucl. Phys. **A489** (1988) 477

[4] C.-H. Yu, J. Gascon, G.B. Hagemann and J.D. Garrett, in Proc. *Exotic Nuclear Spectroscopy*, Ed. W.C. Harris, Plenum Press, New York, 1990, p. 587.

[5] J.L. Salicio, M. Délèze, S. Drissi, J. Kern, S.J. Mannanal, and J.P. Vorlet, Nucl. Phys. **A512** (1990) 109 and S. Drissi, Ziping Li, M. Délèze, J. Kern and J.P. Vorlet, Nucl. Phys. A, in print.

[6] S. André, D. Barnéoud, C. Foin, J. Genevey, J.-A. Pinston, B. Haas, J.P. Vivien and A.J. Kreiner, Z. Phys. **A333** (1989) 333

[7] S. Drissi, J.-Cl. Dousse, V. Ionescu, J. Kern, J.-A. Pinston and D. Barneoud, Nucl. Phys. **A466** (1987) 385

[8] S. Drissi, A. Bruder, J.-Cl. Dousse, V. Ionescu, J. Kern, J.-A. Pinston, S. Andre, D. Barneoud, J. Genevey and H. Frisk, Nucl. Phys. **A451** (1986) 313

[9] S. Drissi, A. Bruder, M. Carlen, J.Cl. Dousse, M. Gasser, J. Kern, S.J. Mannanal, B. Perny, Ch. Rheme, J.L. Salicio, J.P. Vorlet and I. Hamamoto Nucl. Phys. **A543** (1992) 495

[10] S.J. Mannanal, B. Boschung, M.W. Carlen, J.-Cl. Dousse, S.Drissi, P.E. Garrett, J. Kern, B. Perny, Ch. Rheme, J.P. Vorlet, C. Gunther, J. Manns and U. Muller, Nucl. Phys. **A582** (1995) 141; Erratum, Nucl. Phys. **A584** (1995) 758

[11] W. Schmitz, C.X. Yang, H. Hübel, A.P. Byrne, R. Müsseler, N. Singh, K.H. Maier, A. Kuhnert and R. Wyss, Nucl. Phys. **A539** (1992) 112

[12] S. Jósson, J. Lyttkens, L. Carlén, N. Roy, H. Ryde, W. Waluś, J. Kownacki, G.B. Hagemann, B. Harskind, J.D. Garrett, and P.O. Tjøm, Nucl. Phys. A422 (1984) 397, and P. Frandsen, J.D. Garrett, G.B. Hagemann, B. Herskind, M.A. Riley, R. Chapman, J.C. Lisle, J.N. Mo, L. Carlen, J. Lyttkens, H. Ryde, and P.M. Walker, Phys. Lett. **177B** (1986) 287

[13] H.Schnack-Petersen, R. Bengtsson, R.A. Bark, P. Bosetti, A. Brockstedt, H. Carlsson, L.P. Ekström, G.B. Hagemann, B. Harskind, F. Ingebretsen, H.J. Jensen, S. Leoni, A. Nordlund, H. Ryde, P.O. Tjøm and C.X. Yang, Nucl. Phys. **A594** (1995) 175

[14] S. Jonsson, N. Roy, H. Ryde, W. Walus, J. Kownacki, J.D. Garrett, G.B. Hagemann, B. Herskind, R. Bengtsson and S. Aberg, Nucl. Phys. **A449** (1986) 537

[15] H. Xie, Ph.D Thesis, Vanderbilt University, 1990. Unpublished.

[16] E.M. Beck, J.C. Bacelar, M.A. Deleplanque, R.M. Diamond, F.S. Stephens, J.E. Draper, B. Herskind, A. Holm and P.O. Tjøm, Nucl. Phys. **A464** (1987) 472

[17] C. Foin, S. Andre, D. Barneoud, J. Genevey, J.A. Pinston and J. Salicio, Phys. Lett. **159B** (1985) 5

[18] K.P. Blume, H. Hübel, M. Murzel, J. Recht K. Theine, H. Kluge, A. Kuhnert, K.H. Maier, A. Maj, M. Guttormsen and A.P. de Lima, Nucl. Phys. **A464** (1987) 445

[19] H.R. Andrews, E. Hagberg, D. Horn, M.A. Lone, H. Schmeing, D.Ward, P. Taras, J. Gascon, J.C. Waddington, G. Palameta, V.T. Koslowsky and O. Häusser, "Proposal for a National Facility – The 8π Spectrometer", AECL-8329 (1984).

[20] C.J. Gallagher and S.A. Moszkowski, Phys. Rev. **111** (1958) 1282

[21] T. Yamazaki, Nucl. Data **A3** (1967) 1

[22] S.M. Harris, Phys. Rev. **138** (1965) B509

[23] B.R. Mottelson and S.G. Nilsson, Mat. Fys. Dan. Vid. Selsk. **No.8** (1959) 1

[24] H.-Q. Jin, Ph.D thesis, University of Tennessee, Dec., 1991. Unpublished.

[25] D. Hojman, A.J. Kreiner, M. Davidson, J. Davidson, M. Debray, E.W. Cyrulska, P. Pascholati and W.A. Seale, Phys. Rev. **C45** (1992) 90

[26] J.R. Leigh, F.S. Stephens and R.M. Diamond, Phys. Lett. **33B** (1970) 410

[27] W. Reviol, X.Z. Wang and L.L. Riedinger, *et al.*, private communications.

[28] V.P. Janzen, Z.-M. Liu, M.P. Carpenter, L.H. Courtney, H.-Q. Jin, A.J. Larabee, L.L. Riedinger, J.K. Johansson, D.G. Popescu, J.C. Waddington, S. Monaro, S. Pilotte and F. Dönau, Phys. Rev. **C45** (1992) 613

[29] C.-H. Yu, G.B. Hagemann, J.M. Espino, K. Furuno, J.D. Garrett, R. Chapman, D. Clarke, F. Khazaie, J.C. Lisle, J.N. Mo, M. Bergström, L. Carlén, P. Ekström, J. Lyttkens and H. Ryde, Nucl. Phys. **A511** (1990) 157

[30] A. Ikeda and T. Shimano, Phys. Rev. **C42** (1990) 149

[31] R. Bengtsson, H. Frisk, F.R. May, and J.A. Pinston, Nucl. Phys. **A415** (1984) 189

[32] I. Hamamoto, Phys. Lett. **235B** (1990) 221

[33] B. Cederwall, F. Liden, A. Johnson, L. Hildingsson, R. Wyss, B. Fant,S. Juutinen, P. Ahonen, S. Mitarai, J. Mukai, J. Nyberg, I. Ragnarsson and P.B. Semmes, Nucl. Phys. **A542** (1992) 454

[34] M. Matsuzaki, Phys. Lett. **269B** (1991) 23

[35] F. Dönau, Nulc. Phys. **A471** (1987) 469

Figure Captions:

Figure 1: Level scheme of ^{164}Lu established from the ^{149}Sm(^{19}F,4n) and ^{146}Nd(^{23}Na, 5n) reactions at beam energies of 85 MeV and 110 MeV. The uncertain parities and spins are indicated by parentheses, and uncertain transitions are indicated by dashed lines.

Figure 2: Examples of spectra gated on transitions of ^{164} Lu: (2a) Spectrum obtained by gating on the 162.2-keV transition of the yrast band; (2b) Spectrum obtained by gating on the 140.7-keV transition of band 2. Transitions indicated by closed circles are those feeding from band 3. (2c) Spectra obtained by gating on the 222.0-keV transition of band 3. Transitions indicated by down-triangles belong to the yrast band and those indicated by diamonds belong to band 2. Unresolved or contaminant transitions are indicated by stars.

Figure 3: (a) Multiplicity (fold) and (b) Sum-energy spectra obtained by gating on known transitions of ^{163}Lu (shown in thin histograms), ^{165}Lu (shown in medium histograms) and those assinged to ^{164}Lu (shown in thick histograms). The actual experimental fold is equal to the channel number in (a), and the sum-energy is directly proportional to the channel number in (b).

Figure 4. Relative transition probabilities, or $B(M1, I \rightarrow I-1)/B(E2, I \rightarrow I-2)$ ratios, extracted from experimental branching ratios for the yrast band (circles), band 2 (squares) and band 3 (diamonds) of ^{164}Lu. The open and closed symbols represent the $\alpha = 0$ and $\alpha = 1$ signatures, respectively. Calculated $B(M1, I \rightarrow I-1)/B(E2, I \rightarrow I-2)$ ratios for each band are shown in solid curves. See text for more detailed explanations for the calculation and see Table 3 for parameters used in these calculations.

Figure 5. Experimental aligned angular momentum for the six bands in ^{164}Lu. The data are plotted relative to a reference configuration with a moment of inertia given by the Harris[22] parametrization: $I_{ref}(\omega) = \omega J^{(0)} + \omega^3 J^{(1)}$, where $J^{(0)} = 32$ MeV$^{-1}\hbar^2$ and $J^{(1)} = 34$ MeV^{-3} $\hbar^4$.

Figure 6: Comparison of the aligned angular momenta of the yrast band of ^{164}Lu with the proton $9/2^-[514]$ bands in ^{163,165}Lu (ref.[11, 12]) and the neutron low-K $i_{13/2}$ bands in ^{163}Yb

and ^{165}Hf (refs.[2, 18]). The open- and closed symbols for ^{163,165}Lu denote the $(-,-1/2)$ and $(-,+1/2)$ signatures and for ^{164}Lu, the $(-,0)$ and $(-,1)$ signatures, respectively. The data are plotted relative to a reference configuration with a moment of inertia given by the Harris[22] parametrization (see caption for Fig. 5) with $J^{(0)} = 32$ MeV$^{-1}\hbar^2$ and $J^{(1)} = 34$ MeV^{-3} $\hbar^4$.

Figure 7: Comparison of the $I = 12 \rightarrow 10\hbar$ transitions of the yrast bands in the N = 95 and N = 93 odd-odd isotone chains as a function of proton number. Note that the assignment of the 258.2-keV transition as $I = 12 \rightarrow 10\hbar$ in ^{164}Lu fits the exhibited trend.

Figure 8: Single-particle energies as a function of quadrupole deformation, β_2, for protons (left) and neutrons (right) calculated according to the Nilsson model[23] using the Wood-Saxon potentials. The calculations are performed with β_4 and γ deformations fixed at zero. This figure is taken from ref.[24].

Figure 9: Experimental routhians of the yrast band, band 2 and band 3 of ^{164}Lu. The data are plotted relative to a reference configuration with a moment of inertia given by the Harris[22] parametrization (see caption for Fig. 5) with $J^{(0)} = 32$ MeV$^{-1}\hbar^2$ and $J^{(1)} = 34$ MeV^{-3} $\hbar^4$.

Figure 10: $J^{(2)}$ moments of inertia for bands in ^{164}Lu as a function of rotational frequency (right-hand portion) compared with those of ^{163}Lu (left-hand portion). Note the value of $J^{(2)}$ is independent of spins, therefore the uncertain assignment of the spins for bands in ^{164}Lu should not affect the comparison.

Figure 11: Summary of AB neutron band crossing frequencies observed in the yrast bands of even-even Yb isotopes (open circle), the negative-parity bands of odd-A Yb isotopes (closed circles), and the $\pi 9/2^-[514] \otimes \nu 5/2^-[523]$ band (band 2) in odd-odd ^{164}Lu and ^{160,164}Tm(stars). Data for Yb isotopes are taken from ref.[2], and for ^{160,164}Tm are taken from refs.[6, 27].

Figure 12: Cranked Shell Model calculation of the β_2 dependence of the AB neutron crossing frequency for mass $\approx$ 160 nuclei. The calculations were performed with γ and β_4 fixed at values predicted by the TRS for these nuclei. The TRS prediction of β_2 values for ^{160,164}Tm, ^{164}Lu

and ^{163,165}Yb are indicated by arrows.

Figure 13: Energy signature splittings, $\Delta E(I)$ defined by Eq. (3) of subsection 3.2, as a function of spin for the three strongly coupled bands of ^{164}Lu in comparison with related bands in ^{163}Lu and ^{165}Lu. The open and closed symbols for ^{164}Lu represent the $\alpha = 0$ and $\alpha = 1$ signatures, respectively, and for ^{163,165}Lu represent the $\alpha = -1/2$ and $\alpha = 1/2$ signatures respectively.

Table 1: Data Table for ^{164}Lu

E_γ(keV) [a]	$I_i^\pi \rightarrow I_f^\pi$ [b]	R_{DCO} [c]	I_γ^{rel} [d]	λ [e]	$\frac{B(M1,I\rightarrow I-1)}{B(E2,I\rightarrow I-2)}$ [f]
		Yrast Band, $\alpha = 0$			
258.2	$(12^-) \rightarrow (10^-)$	0.71± 0.05	53± 11	0.12 ± 0.01	1.52 ± 0.02
165.2	$(12^-) \rightarrow (11^-)$	0.71± 0.03	500± 43		
399.0	$(14^-) \rightarrow (12^-)$	0.94± 0.10	185± 40	0.41 ± 0.05	1.29 ± 0.14
236.8	$(14^-) \rightarrow (13^-)$	0.68± 0.04	439± 25		
510.9	$(16^-) \rightarrow (14^-)$	0.85± 0.07	245± 22	0.95 ± 0.07	1.10 ± 0.08
284.6	$(16^-) \rightarrow (15^-)$	0.64± 0.03	305± 20		
596.5	$(18^-) \rightarrow (16^-)$	0.70± 0.07	280± 21	1.53 ± 0.11	1.12 ± 0.08
312.7	$(18^-) \rightarrow (17^-)$	0.68± 0.04	177± 10		
656.5	$(20^-) \rightarrow (18^-)$	1.03± 0.10	233± 10	1.81 ± 0.14	1.36 ± 0.10
324.9	$(20^-) \rightarrow (19^-)$	0.71± 0.05	132± 10		
686.7	$(22^-) \rightarrow (20^-)$	0.97± 0.06	199± 10	2.92 ± 0.24	1.07 ± 0.09
323.0	$(22^-) \rightarrow (21^-)$	0.60± 0.04	92± 10		
697.1	$(24^-) \rightarrow (22^-)$	0.92± 0.12	142± 10	3.14 ± 0.24	1.11 ± 0.09
320.0	$(24^-) \rightarrow (23^-)$	0.58± 0.08	58± 7		
722.8	$(26^-) \rightarrow (24^-)$	1.01± 0.24	90± 12	2.64 ± 0.21	1.39 ± 0.11
334.4	$(26^-) \rightarrow (25^-)$	0.69± 0.10	43± 6		
774.8	$(28^-) \rightarrow (26^-)$	1.30± 0.20	90± 6	2.82 ± 0.29	1.46 ± 0.15
361.2	$(28^-) \rightarrow (27^-)$	0.70± 0.12	31± 7		
840.9	$(30^-) \rightarrow (28^-)$		76± 7	2.18 ± 0.28	2.22 ± 0.28
391.8	$(30^-) \rightarrow (29^-)$		18± 4		
910.4	$(32^-) \rightarrow (30^-)$		28± 6		
418.3	$(32^-) \rightarrow (31^-)$		8± 3		
974.7	$(34^-) \rightarrow (32^-)$		26± 6		
1028	$(36^-) \rightarrow (34^-)$		25± 5		
1090	$(38^-) \rightarrow (36^-)$		11± 3		

Table 1: Data Table for ^{164}Lu (continued)

E_γ(keV) [a]	$I_i^\pi \rightarrow I_f^\pi$ [b]	R_{DCO} [c]	I_γ^{rel} [d]	λ [e]	$\frac{B(M1,I\rightarrow I-1)}{B(E2,I\rightarrow I-2)}$ [f]
		Yrast Band, $\alpha = 1$			
93.0	$(11^-) \rightarrow (10^-)$	0.41± 0.09	133± 15		
327.4	$(13^-) \rightarrow (11^-)$	0.91± 0.07	170± 9	0.46 ± 0.05	1.34 ± 0.15
162.2	$(13^-) \rightarrow (12^-)$	0.68± 0.03	355± 26		
463.0	$(15^-) \rightarrow (13^-)$	1.08± 0.04	332± 25	1.12 ± 0.13	1.15 ± 0.13
226.3	$(15^-) \rightarrow (14^-)$	0.78± 0.03	317± 15		
568.4	$(17^-) \rightarrow (15^-)$	1.08± 0.07	308± 15	1.74 ± 0.13	1.04 ± 0.08
283.8	$(17^-) \rightarrow (16^-)$	0.68± 0.04	189± 17		
644.4	$(19^-) \rightarrow (17^-)$	0.91± 0.06	269± 17	1.97 ± 0.17	1.08 ± 0.09
331.6	$(19^-) \rightarrow (18^-)$	0.63± 0.10	123± 9		
688.6	$(21^-) \rightarrow (19^-)$	0.98± 0.07	215± 9	2.23 ± 0.24	1.00 ± 0.11
363.7	$(21^-) \rightarrow (20^-)$	0.56± 0.05	95± 9		
700.1	$(23^-) \rightarrow (21^-)$	1.07± 0.19	134± 9	1.63 ± 0.13	1.33 ± 0.11
377.1	$(23^-) \rightarrow (22^-)$	0.40± 0.07	78± 9		
708.4	$(25^-) \rightarrow (23^-)$	1.02± 0.16	82± 7	1.84 ± 0.17	1.15 ± 0.11
388.4	$(25^-) \rightarrow (24^-)$	0.49± 0.12	54± 8		
747.9	$(27^-) \rightarrow (25^-)$	1.42± 0.25	62± 6	1.64 ± 0.15	1.40 ± 0.13
413.5	$(27^-) \rightarrow (26^-)$	0.56± 0.11	35± 5		
810.4	$(29^-) \rightarrow (27^-)$		59± 6	1.39 ± 0.21	1.93 ± 0.30
449.1	$(29^-) \rightarrow (28^-)$		19± 7		
883.8	$(31^-) \rightarrow (31^-)$		32± 7		
492.0	$(31^-) \rightarrow (30^-)$		20± 8		
960.6	$(33^-) \rightarrow (31^-)$		27± 7		
1035	$(35^-) \rightarrow (28^-)$		26± 10		
1084	$(37^-) \rightarrow (35^-)$		15± 4		
1114	$(39^-) \rightarrow (37^-)$		9± 4		

Tabel 1: Data Table for ^{164}Lu (continued)

E_γ(keV) [a]	$I_i^\pi \rightarrow I_f^\pi$ [b]	R_{DCO} [c]	I_γ^{rel} [d]	λ [e]	$\frac{B(M1,I\rightarrow I-1)}{B(E2,I\rightarrow I-2)}$ [f]
		Transitions at the Yrast Bandhead			
101.0	$(10^-) \rightarrow$		8± 5		
161.5	$(10^-) \rightarrow$	0.9± 0.1	154± 40		
142.2			20± 4		
171.7	$(10^-) \rightarrow$	0.74± 0.05	91± 21		
184.3	$(10^-) \rightarrow$	0.73± 0.04	45± 12		
		Band 2, $\alpha = 0$			
118.8	$(10^+) \rightarrow (8^+)$	1.04± 0.12	16± 7		
103.6	$(10^+) \rightarrow (9^+)$	0.74± 0.08	36± 7		
308.7	$(12^+) \rightarrow (10^+)$	0.87± 0.05	66± 6	1.12 ± 0.13	0.37 ± 0.04
168.0	$(12^+) \rightarrow (11^+)$	0.76± 0.04	75± 12		
434.8	$(14^+) \rightarrow (12^+)$	0.96± 0.07	134± 19	2.38 ± 0.29	0.40 ± 0.05
224.5	$(14^+) \rightarrow (13^+)$	0.75± 0.11	73± 10		
533.8	$(16^+) \rightarrow (14^+)$	1.08± 0.07	141± 10	3.74 ± 0.60	0.42 ± 0.07
266.6	$(16^+) \rightarrow (15^+)$	0.69± 0.04	48± 11		
605.7	$(18^+) \rightarrow (16^+)$	0.92± 0.06	149± 11	6.51 ± 0.74	0.33 ± 0.04
298.1	$(18^+) \rightarrow (17^+)$	0.75± 0.05	25± 14		
632.9	$(20^+) \rightarrow (18^+)$	1.12± 0.07	98± 14	2.45 ± 0.79	1.00 ± 0.32
306.7	$(20^+) \rightarrow (19^+)$	0.76± 0.11	29± 9		
586.8	$(22^+) \rightarrow (20^+)$	1.25± 0.28	33± 9	2.12 ± 0.22	0.94 ± 0.10
289.2	$(22^+) \rightarrow (21^+)$	0.40± 0.06	29± 6		

Table 1: Data Table for ^{164}Lu (continued)

E_γ(keV) [a]	$I_i^\pi \rightarrow I_f^\pi$ [b]	R_{DCO} [c]	I_γ^{rel} [d]	λ [e]	$\frac{B(M1,I\rightarrow I-1)}{B(E2,I\rightarrow I-2)}$ [f]
627.9	$(24^+) \rightarrow (22^+)$	0.83± 0.09	50± 5	2.56 ± 0.20	0.83 ± 0.07
317.4	$(24^+) \rightarrow (23^+)$	0.67± 0.17	24± 5		
700.4	$(26^+) \rightarrow (24^+)$	1.02± 0.16	49± 5	3.78 ± 0.37	0.70 ± 0.07
354.2	$(26^+) \rightarrow (25^+)$		15± 4		
778.5	$(28^+) \rightarrow (26^+)$		31± 6		
395	$(28^+) \rightarrow (27^+)$		13± 6		
879.1	$(30^+) \rightarrow (28^+)$		16± 5		
960.6	$(32^+) \rightarrow (30^+)$		9± 3		
1004	$(34^+) \rightarrow (32^+)$		12± 4		
	Band 2, $\alpha = 1$				
244.5	$(11^+) \rightarrow (9^+)$		17± 10		
140.7	$(11^+) \rightarrow (10^+)$	0.64± 0.07	49± 14		
378.4	$(13^+) \rightarrow (11^+)$	0.80± 0.05	88± 6	1.28 ± 0.15	0.45 ± 0.05
210.3	$(13^+) \rightarrow (12^+)$	0.70± 0.03	84± 14		
491.7	$(15^+) \rightarrow (13^+)$	0.93± 0.04	123± 14	1.99 ± 0.16	0.53 ± 0.04
267.2	$(15^+) \rightarrow (14^+)$	0.80± 0.03	60± 9		
574.2	$(17^+) \rightarrow (15^+)$	0.97± 0.05	113± 13	2.91 ± 0.69	0.52 ± 0.12
307.6	$(17^+) \rightarrow (16^+)$	0.75± 0.04	43± 9		
624.4	$(19^+) \rightarrow (17^+)$	1.30± 0.03	110± 14	1.77 ± 0.18	1.06 ± 0.11
326.3	$(19^+) \rightarrow (18^+)$	0.58± 0.06	52± 12		
604.2	$(21^+) \rightarrow (19^+)$	0.90± 0.05	73± 9	g)	g)
297.6	$(21^+) \rightarrow (20^+)$	0.59± 0.06	33± 6		
599.7	$(23^+) \rightarrow (21^+)$	0.90± 0.08	53± 10	2.42 ± 0.65	0.75 ± 0.21
310.5	$(23^+) \rightarrow (22^+)$		25± 5		
663.6	$(25^+) \rightarrow (23^+)$	0.78± 0.14	41± 7	2.20 ± 0.20	0.98 ± 0.09
346.2	$(25^+) \rightarrow (24^+)$		18± 4		

Table 1: Data Table for ^{164}Lu (continued)

E_γ(keV) [a]	$I_i^\pi \rightarrow I_f^\pi$ [b]	R_{DCO} [c]	I_γ^{rel} [d]	λ [e]	$\frac{B(M1,I\rightarrow I-1)}{B(E2,I\rightarrow I-2)}$ [f]
737.5	$(27^+) \rightarrow (25^+)$		28± 6		
383.3	$(27^+) \rightarrow (26^+)$		12± 4		
833.1	$(29^+) \rightarrow (27^+)$		31± 7		
922	$31^+ \rightarrow 29^+$		12± 4		
		Band 3, $\alpha = 0$			
964.7	$(16^+) \rightarrow (15^-)$	0.70± 0.32	51± 12		
648.0	$(18^+) \rightarrow (16^+)$	1.02± 0.21	40± 8		
390.7	$(18^+) \rightarrow (16^+)$		9± 4		
206.4	$(18^+) \rightarrow (17^+)$		28± 5		
460.1	$(20^+) \rightarrow (18^+)$	0.93± 0.09	39± 8	} 0.57 ± 0.04	1.86 ± 0.11
238.1	$(20^+) \rightarrow (19^+)$	0.72± 0.04	64± 11		
550.1	$(22^+) \rightarrow (20^+)$	1.02± 0.18	33± 8	h)	h)
283.4	$(22^+) \rightarrow (21^+)$	0.56± 0.02	54± 9		
659.5	$(24^+) \rightarrow (22^+)$	1.26± 0.21	52± 10	} 1.45 ± 0.20	1.55 ± 0.15
337.7	$(24^+) \rightarrow (23^+)$	0.80± 0.10	36± 7		
760.6	$(26^+) \rightarrow (24^+)$	1.06± 0.37	49± 9	} 1.94 ± 0.11	1.51 ± 0.09
392.1	$(26^+) \rightarrow (25^+)$	0.75± 0.15	25± 5		
818.1	$(28^+) \rightarrow (26^+)$	0.87± 0.40	34± 7	} 2.20 ± 0.15	1.58 ± 0.11
418.6	$(28^+) \rightarrow (27^+)$		12± 4		
850.5	$(30^+) \rightarrow (28^+)$	1.03± 0.24	41± 8		
432.6	$(30^+) \rightarrow (29^+)$		15± 4		
897.9	$(32^+) \rightarrow (30^+)$		25± 6		
457.9	$(32^+) \rightarrow (31^+)$		8± 4		
952.4	$(34^+) \rightarrow (32^+)$		21± 5		
1012	$(36^+) \rightarrow (34^+)$		20± 5		
1065	$(38^+) \rightarrow (36^+)$		12± 5		

Table 1: Data Table for ^{164}Lu (continued)

E_γ(keV) [a]	$I_i^\pi \rightarrow I_f^\pi$ [b]	R_{DCO} [c]	I_γ^{rel} [d]	λ [e]	$\frac{B(M1,I\rightarrow I-1)}{B(E2,I\rightarrow I-2)}$ [f]
		Band 3, $\alpha = 1$			
184.2	$(17^+) \rightarrow (16^+)$	0.77± 0.55	21± 5		
864.7	$(17^+) \rightarrow (16^-)$	0.64± 0.24	47± 10		
428.4	$(19^+) \rightarrow (17^+)$	0.64± 0.11	29± 5		
222.0	$(19^+) \rightarrow (18^+)$		35± 7		
504.9	$(21^+) \rightarrow (19^+)$	1.20± 0.14	40± 8	} 0.73 ± 0.06	1.65 ± 0.14
266.8	$(21^+) \rightarrow (20^+)$	0.73± 0.03	54± 9		
605.2	$(23^+) \rightarrow (21^+)$	0.95± 0.09	69± 13	} 1.29 ± 0.12	1.30 ± 0.10
321.8	$(23^+) \rightarrow (22^+)$	0.74± 0.04	51± 9		
706.2	$(25^+) \rightarrow (23^+)$	0.74± 0.13	54± 9	} 1.58 ± 0.09	1.54 ± 0.08
368.5	$(25^+) \rightarrow (24^+)$	0.50± 0.11	29± 5		
791.6	$(27^+) \rightarrow (25^+)$	0.85± 0.30	35± 8		
399.5	$(27^+) \rightarrow (26^+)$		23± 5		
836.6	$(29^+) \rightarrow (27^+)$	1.07± 0.19	49± 10		
417.9	$(29^+) \rightarrow (28^+)$		9± 4		
872.9	$(31^+) \rightarrow (29^+)$		24± 6		
440.1	$(31^+) \rightarrow (30^+)$		10± 4		
918.3	$(33^+) \rightarrow (31^+)$		16± 5		
460.5	$(33^+) \rightarrow (32^+)$		9± 4		
969.5	$(35^+) \rightarrow (33^+)$		18± 4		
1018	$(37^+) \rightarrow (35^+)$		22± 5		
1069	$(39^+) \rightarrow (37^+)$		12± 4		

Table 1: Data Table for ^{164}Lu (continued)

E_γ(keV) [a]	$I_i^\pi \rightarrow I_f^\pi$ [b]	I_γ^{rel} [c]
	Band 4	
462.1	(12) → (10)	30± 6
551.3	(14) → (12)	33± 5
616.9	(16) → (14)	37± 4
662.8	(18) → (16)	26± 7
691.7	(20) → (18)	15± 6
	Band 5	
152.8	(9) → (8)	11± 6
401.2	(11) → (9)	64± 6
505.7	(13) → (11)	59± 9
585.3	(15) → (13)	60± 8
632.8	(17) → (15)	43± 7
648.9	(19) → (17)	35± 6
672.8	(21) → (19)	15± 5
	Band 6	
159.3	(8) → (6)	16± 6
357.5	(10) → (8)	25± 7
471.9	(12) → (10)	24± 6
559.8	(14) → (12)	18± 6
618.8	(16) → (14)	15± 6
651.6	(18) → (16)	16± 5
669.5	(20) → (18)	12± 5

a) Accurate to 0.3 keV for most transitions. For weak or contaminant transitions, accurate to 0.5 or 1 keV.

b) Spins and parities for the yrast band, band 2 and band 3 are assigned based on systematic trend and tentative connecting transitions between these three bands. No parity is assigned to band 4, 5 and 6. The spin assignment for band 4, 5 and 6 are extremely tentative.

c) Branching ratios measured from spectra obtained by gating on transitions above the transition of interest. For higher spin states, λ values are also determined from spectra gated on low-spin transitions. Some values are obtained by averaging the results from the two methods.

d) Relative gamma-ray intensities normalized to the 165.2-keV transition ($\equiv$ 500) in the yrast band.

e) DCO ratios obtained from the sum of spectra gated on clean, $\Delta I = 2$ transitions above the transition of interest.

f) Assuming mixing ratio $\delta = 0$. In most cases the error induced by this assumption is negligible compared to the errors induced by the branching ratios.

g) Doublet transition makes it difficult to extract the branching ratio.

h) The 283.4-keV transition is contaminated by the very strong 283-keV from the yrast band, no reliable branching ratio can be extracted.

Table 2: The nomenclature for quasipartice configurations used in the present work

Neutrons		Protons[a)]	
configuration[a)]	label	configuration	label
$(+,+\frac{1}{2})_1$	A	$(-,-\frac{1}{2})_1$	A_p
$(+,-\frac{1}{2})_1$	B	$(-,+\frac{1}{2})_1$	B_p
$(+,+\frac{1}{2})_2$	C	$(-,-\frac{1}{2})_2$	C_p
$(+,-\frac{1}{2})_2$	D	$(-,+\frac{1}{2})_2$	D_p
$(-,+\frac{1}{2})_1$	E	$(+,-\frac{1}{2})_1$	E_p
$(-,-\frac{1}{2})_1$	F	$(+,+\frac{1}{2})_1$	F_p

a) The nth lowest excitation of a specific configuration with signature, α, and parity, π, is denoted by $(\pi,\alpha)_n$.

Table 3: Parameters used for calculation of B(M1)/B(E2) ratios

	Yrast Band	Band 2	Band 3
K	6.00	6.00	9.00
g_R	0.21	0.43	0.30
g_p	1.35	1.35	1.35
g_n	-0.33	0.26	-0.30
g_a	-0.33	-0.33	-0.33
i_p	1.00	1.00	1.00
i_n	5.00	0.50	0.01
i_a	6.90	6.90	8.00
k_p	4.50	4.50	4.50
Q_0	5.80	5.80	5.00

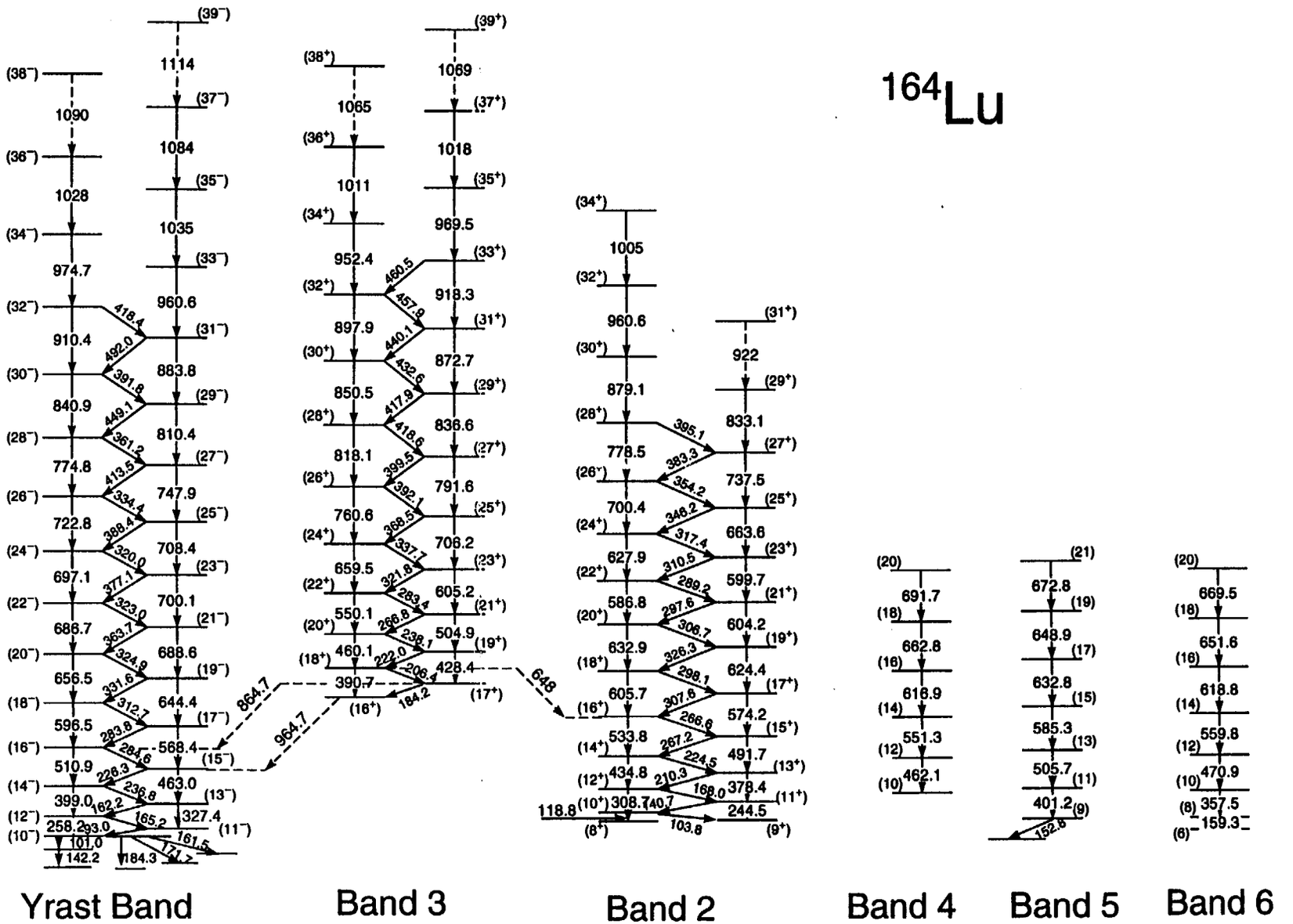

X.-H. Wang et al, Fig. 1

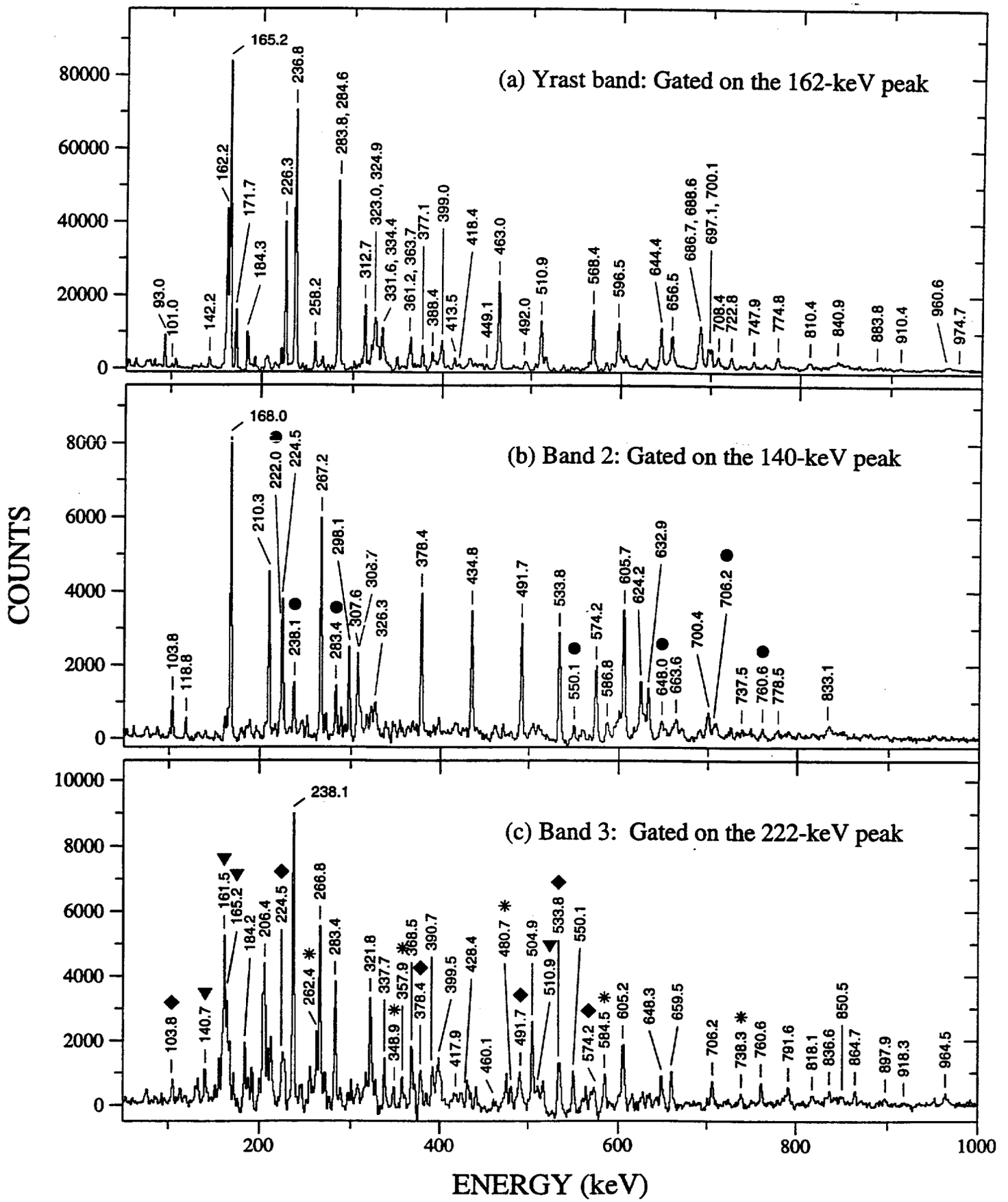

X.-H. Wang et al., Fig. 2

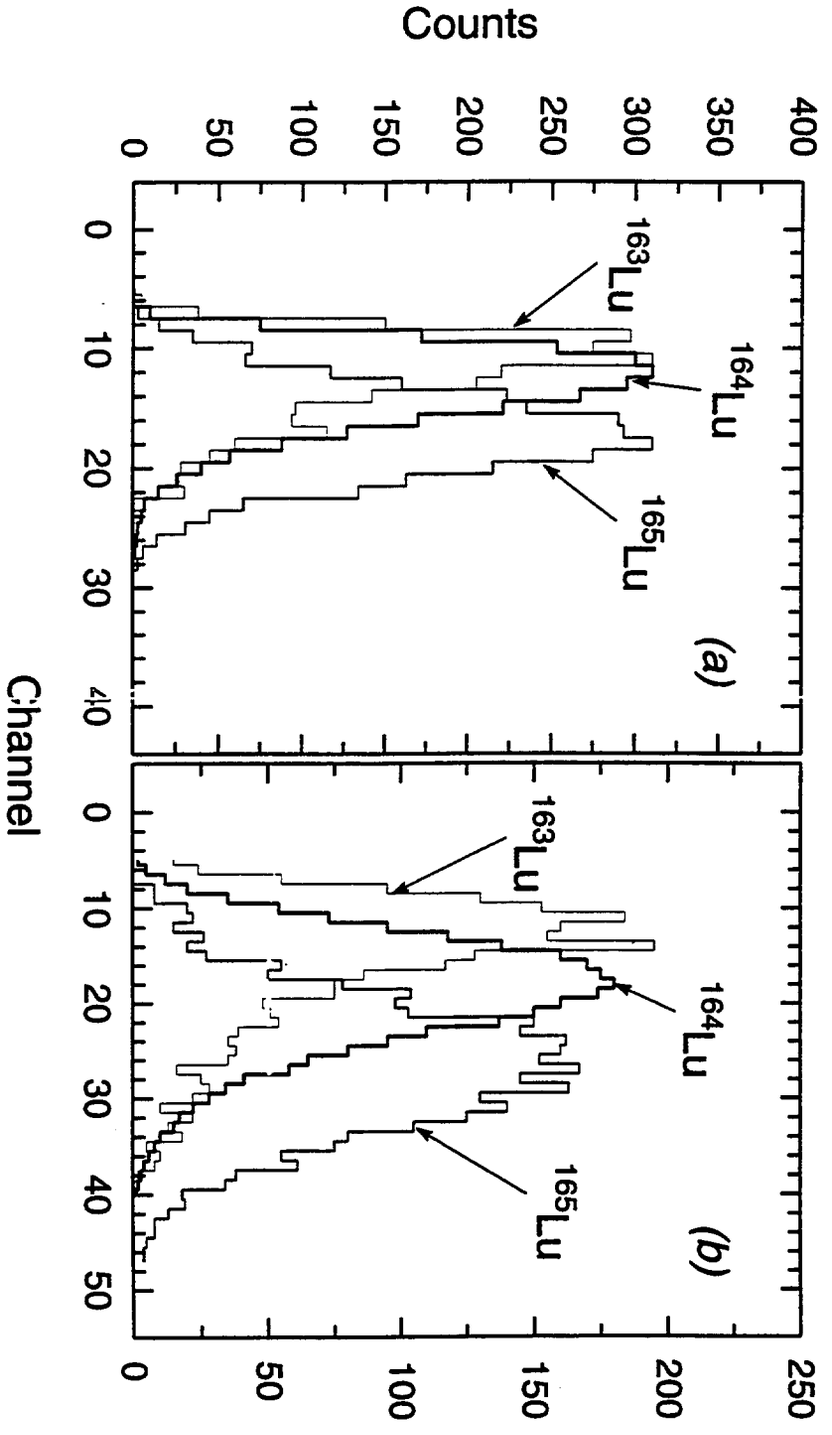
Counts
Fold
Sum-energy
Channel
^{163}Lu
^{164}Lu
^{165}Lu
(a)
(b)

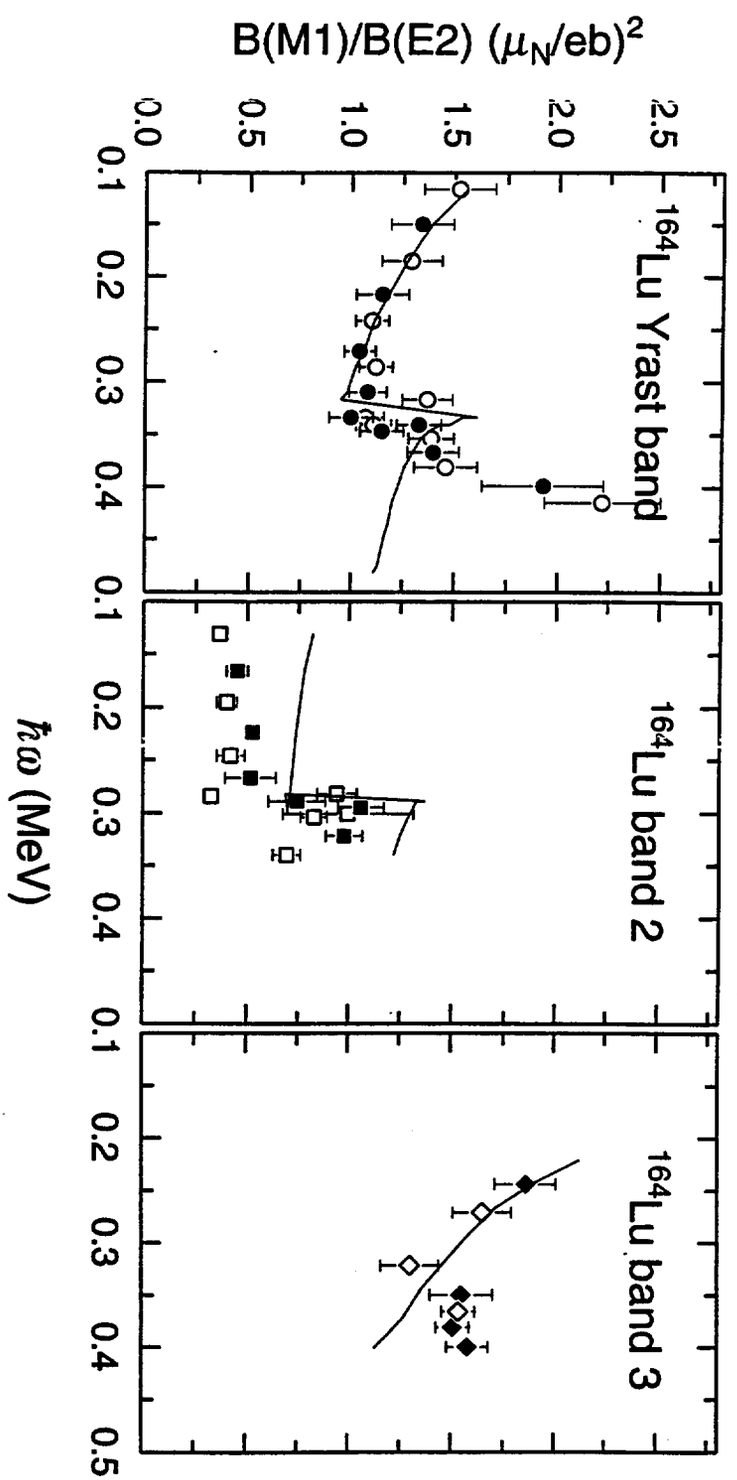
B(M1)/B(E2) (μ_N/eb)^2
$\hbar\omega$ (MeV)
^{164}Lu Yrast band
^{164}Lu band 2
^{164}Lu band 3

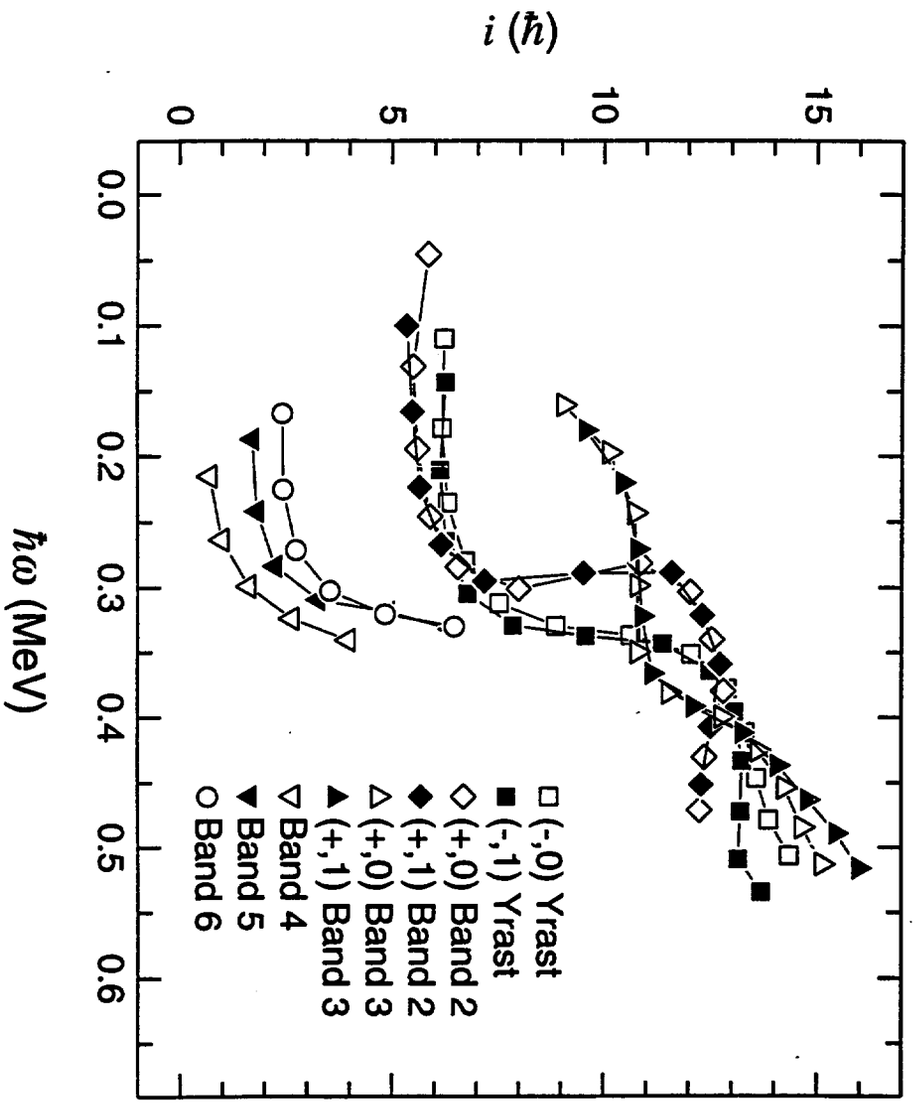
^{164}Lu
i ($\hbar$)
$\hbar\omega$ (MeV)
0
5
10
15
0.0
0.1
0.2
0.3
0.4
0.5
0.6
(-,0) Yrast
(-,1) Yrast
(+,0) Band 2
(+,1) Band 2
(+,0) Band 3
(+,1) Band 3
Band 4
Band 5
Band 6

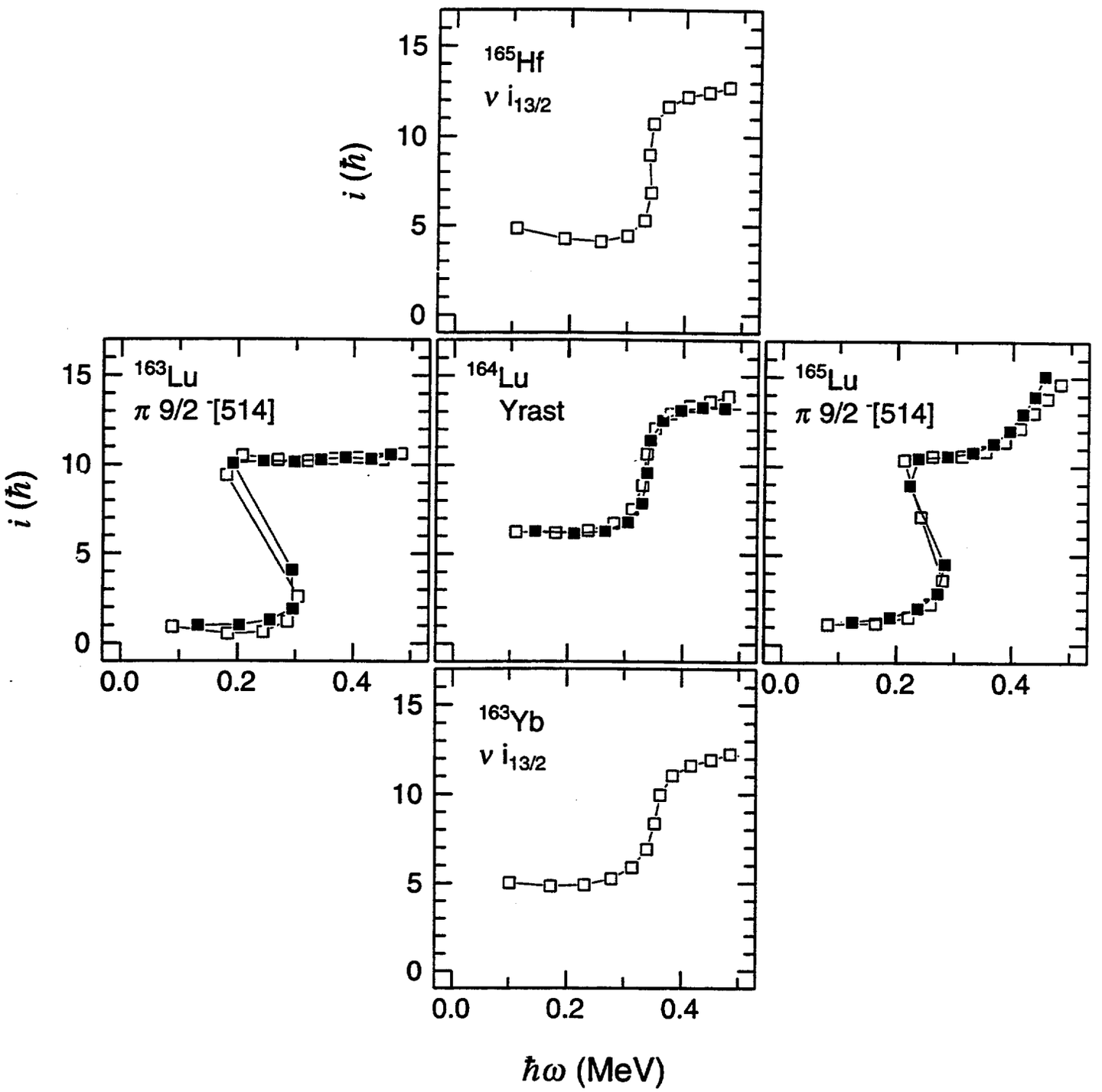

X.-H. Wang, et al, Fig. 6

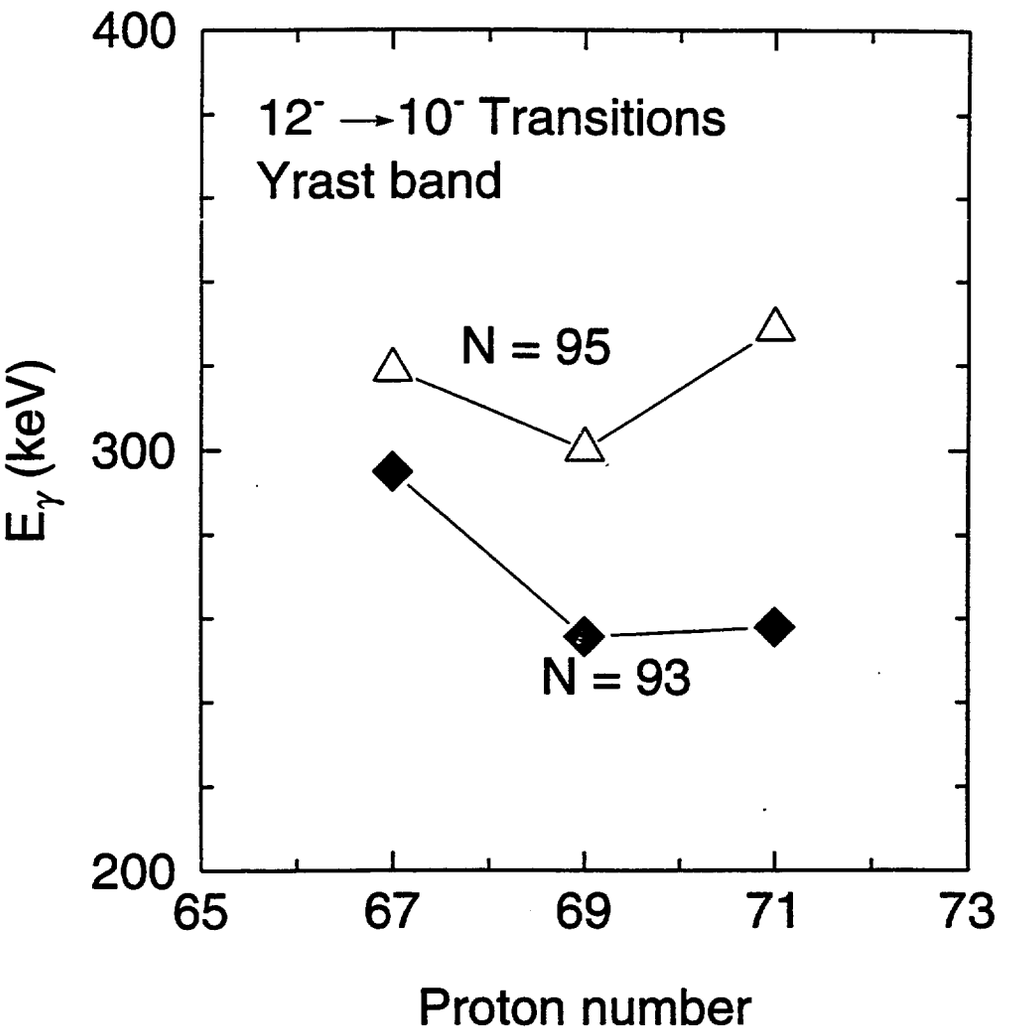

X.-H. Wang, et al, Fig. 7

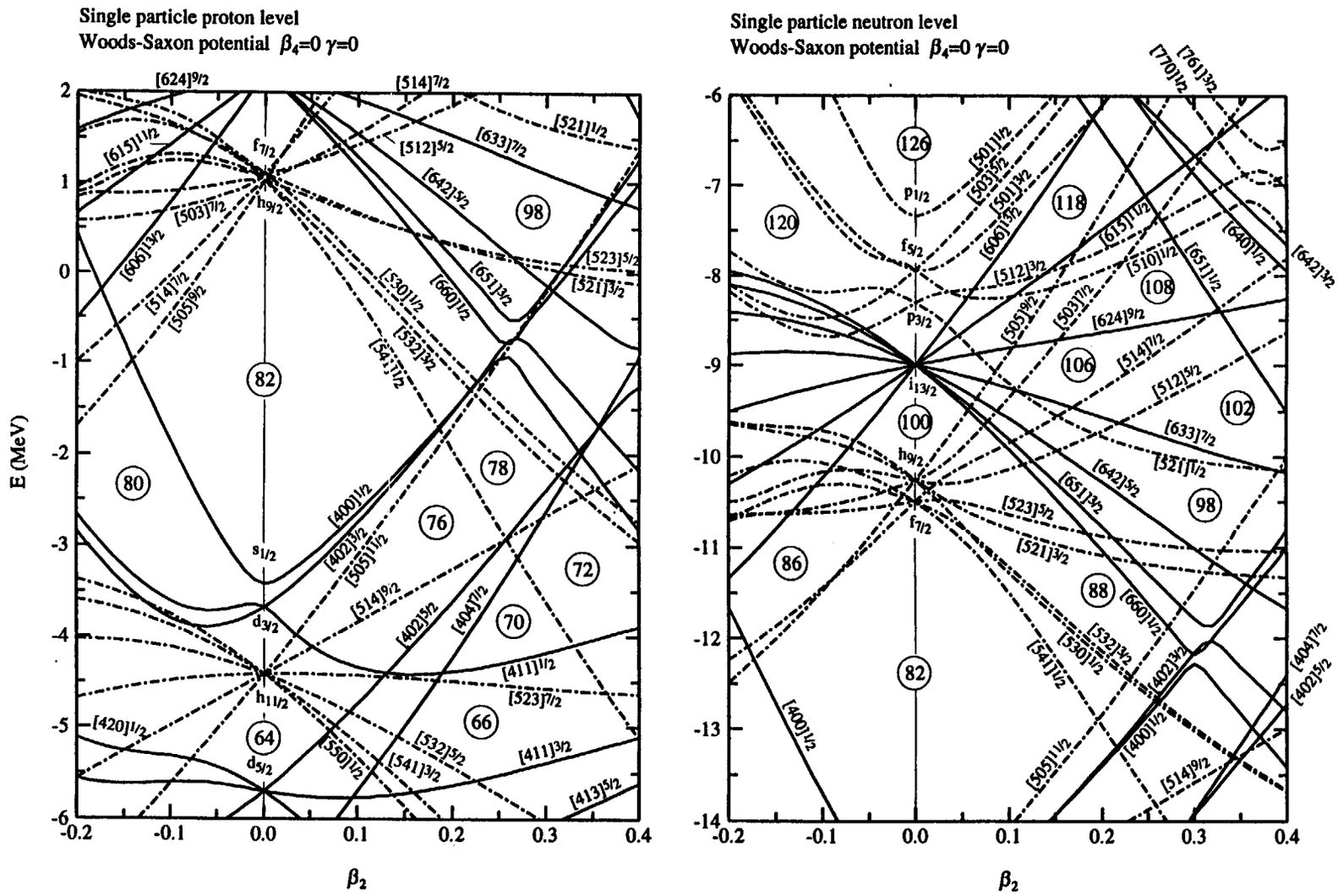

X.-H. Wang, et al, Fig. 8

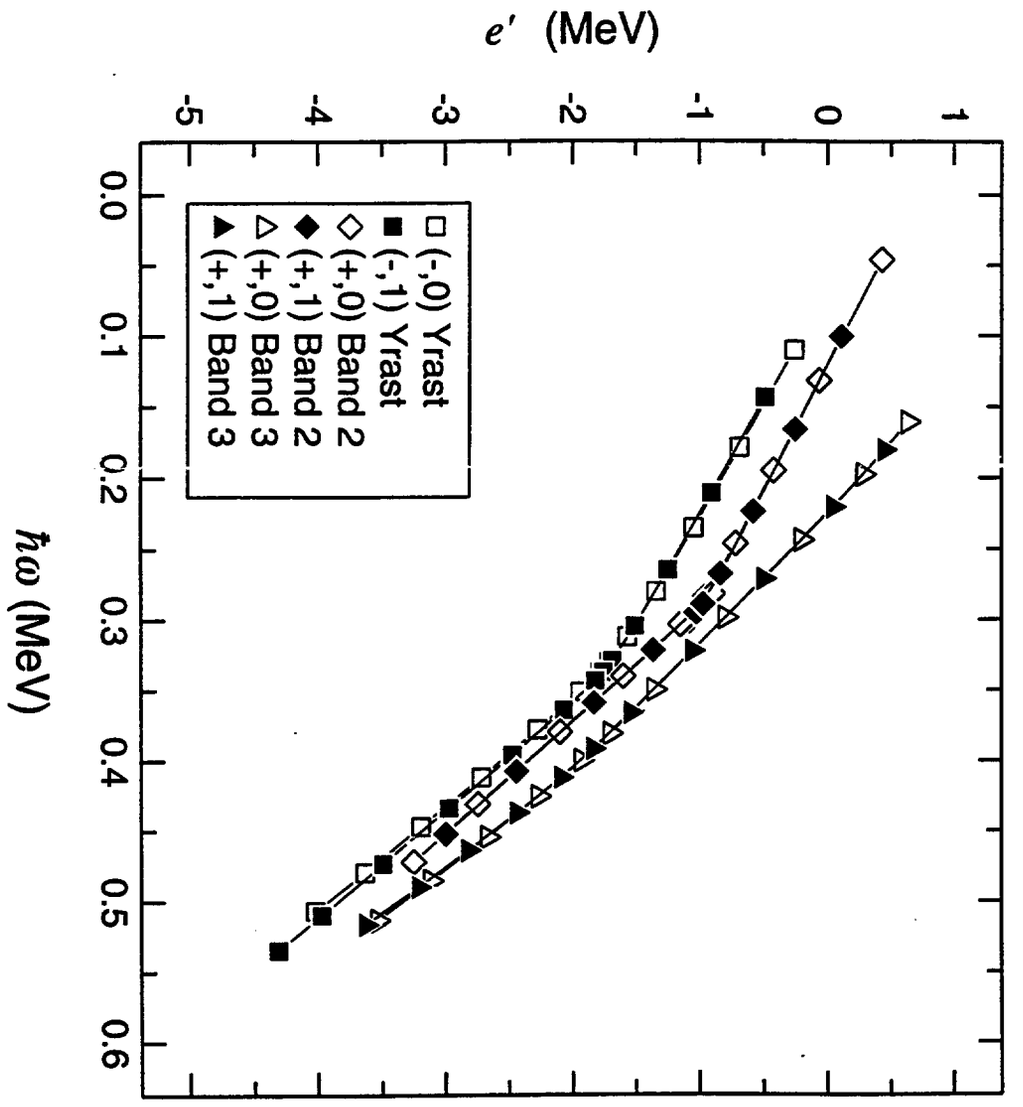
^{164}Lu
e' (MeV)
$\hbar\omega$ (MeV)
(-,0) Yrast
(-,1) Yrast
(+,0) Band 2
(+,1) Band 2
(+,0) Band 3
(+,1) Band 3

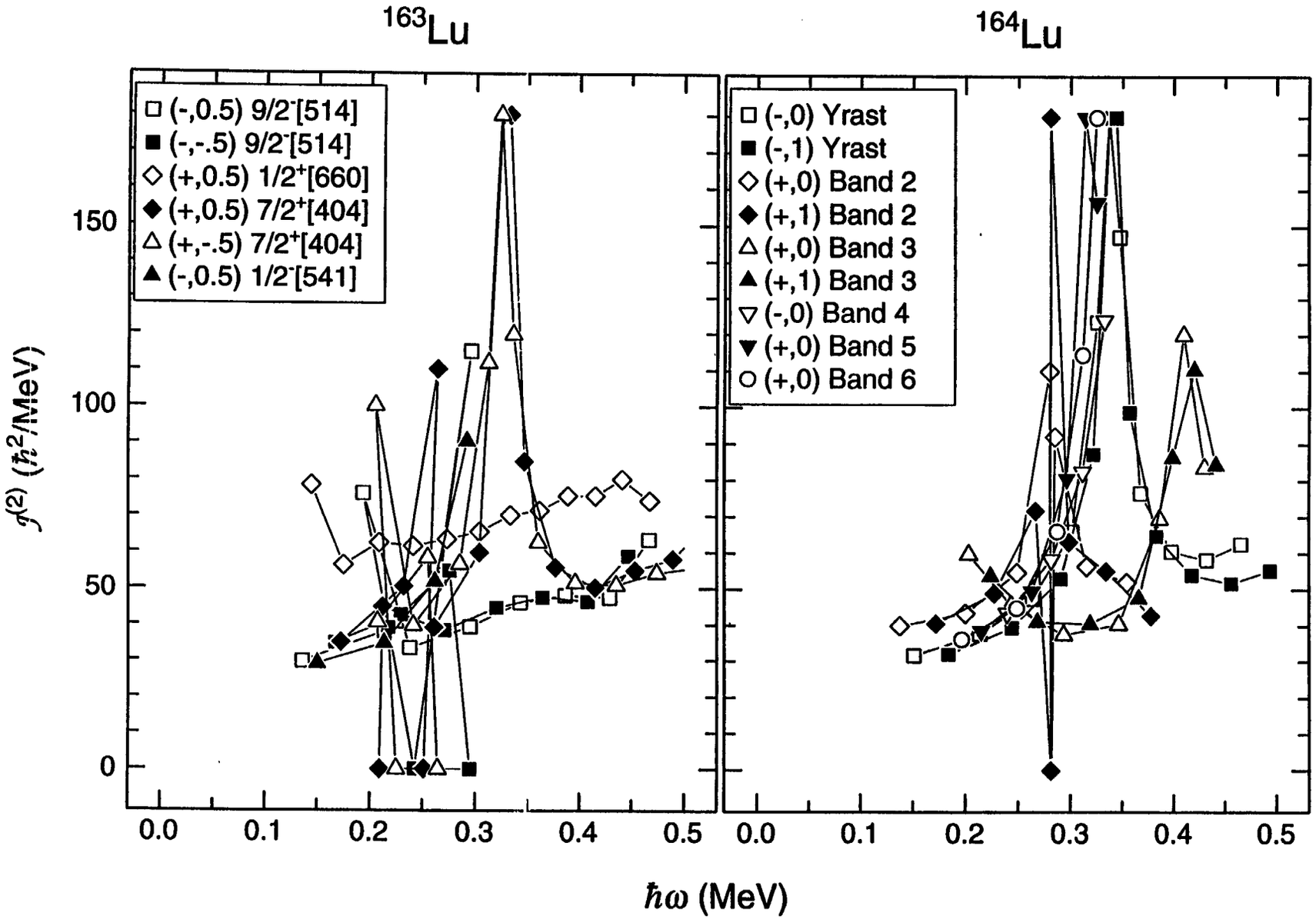

X.H. Wang, et al, Fig. 10

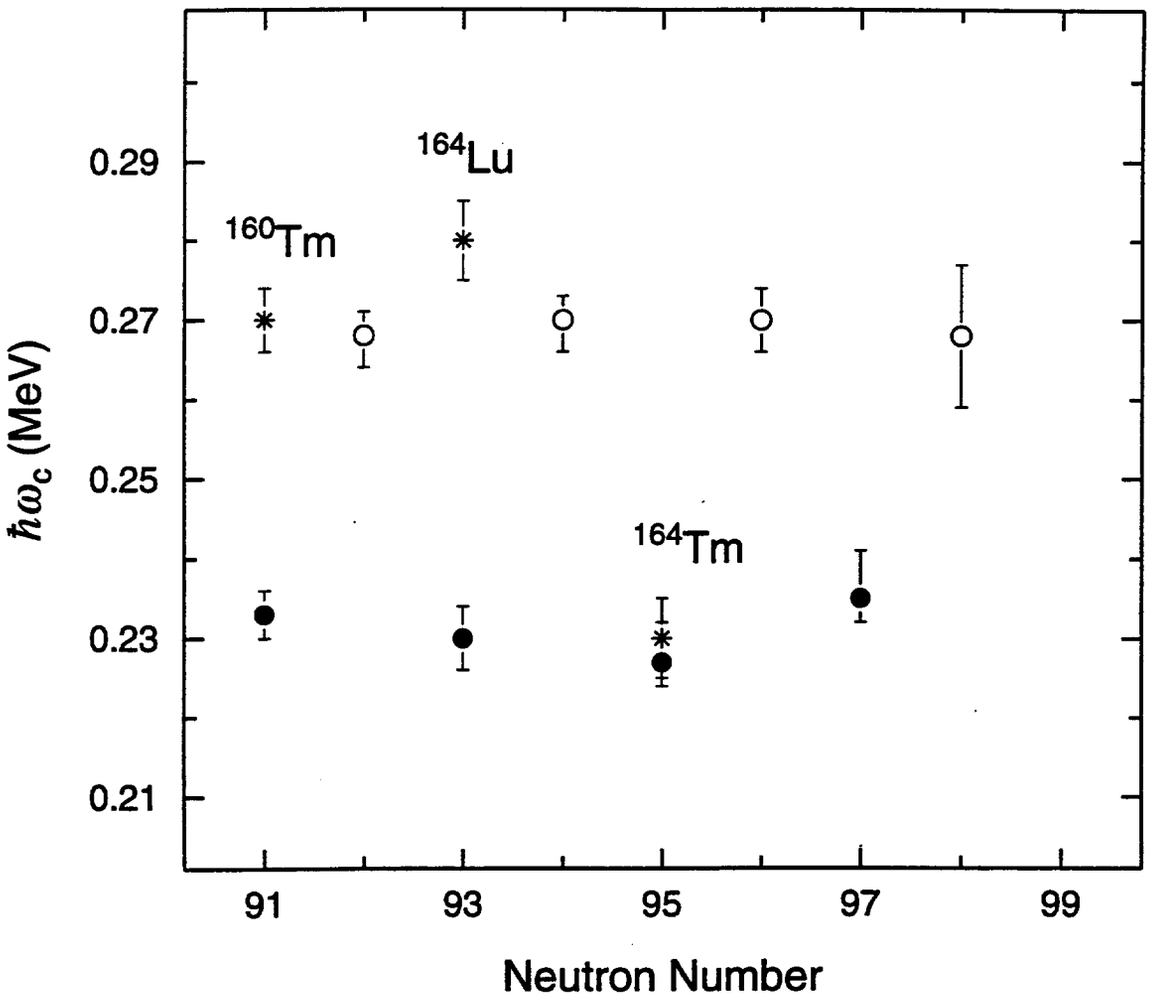

X.-H. Wang, et al, Fig. 11

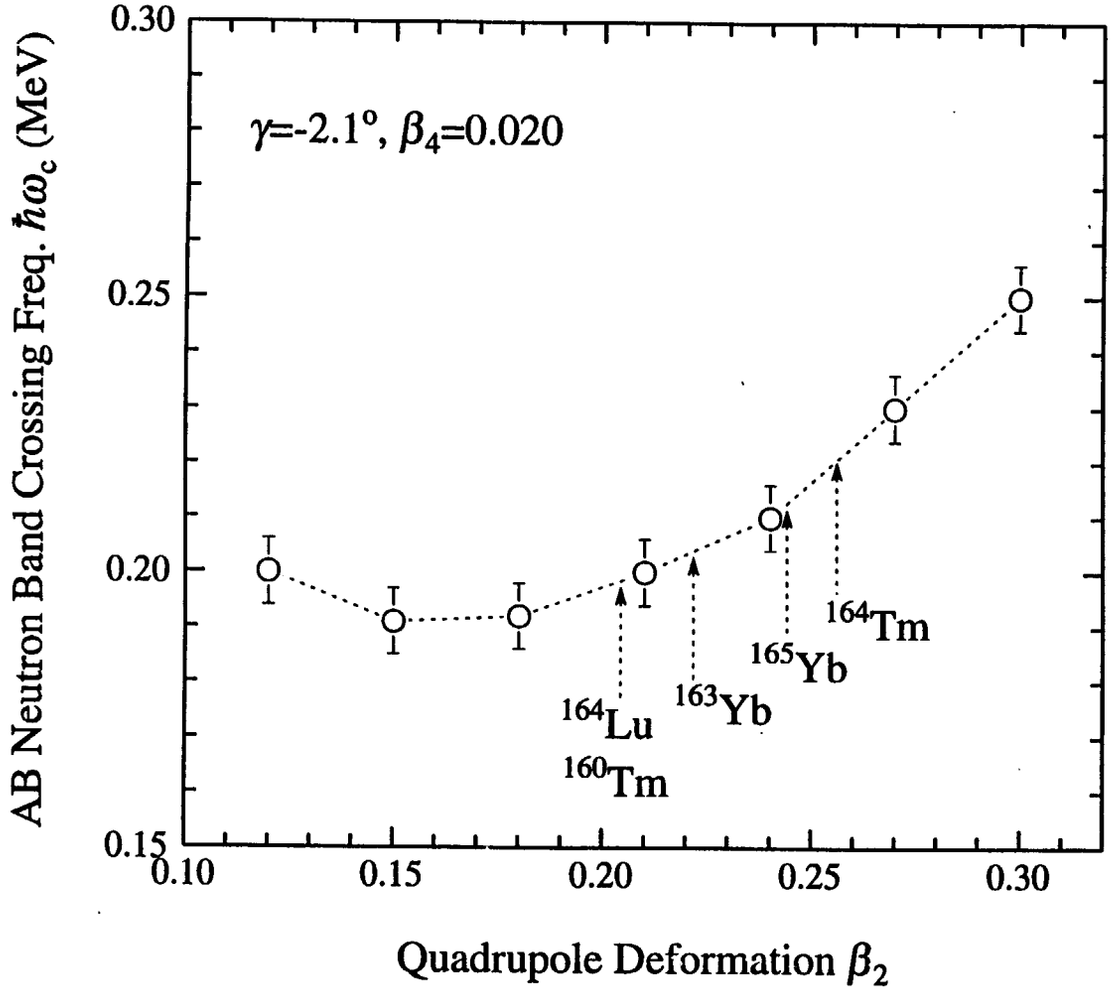

X.-H. Wang, et al, Fig. 12

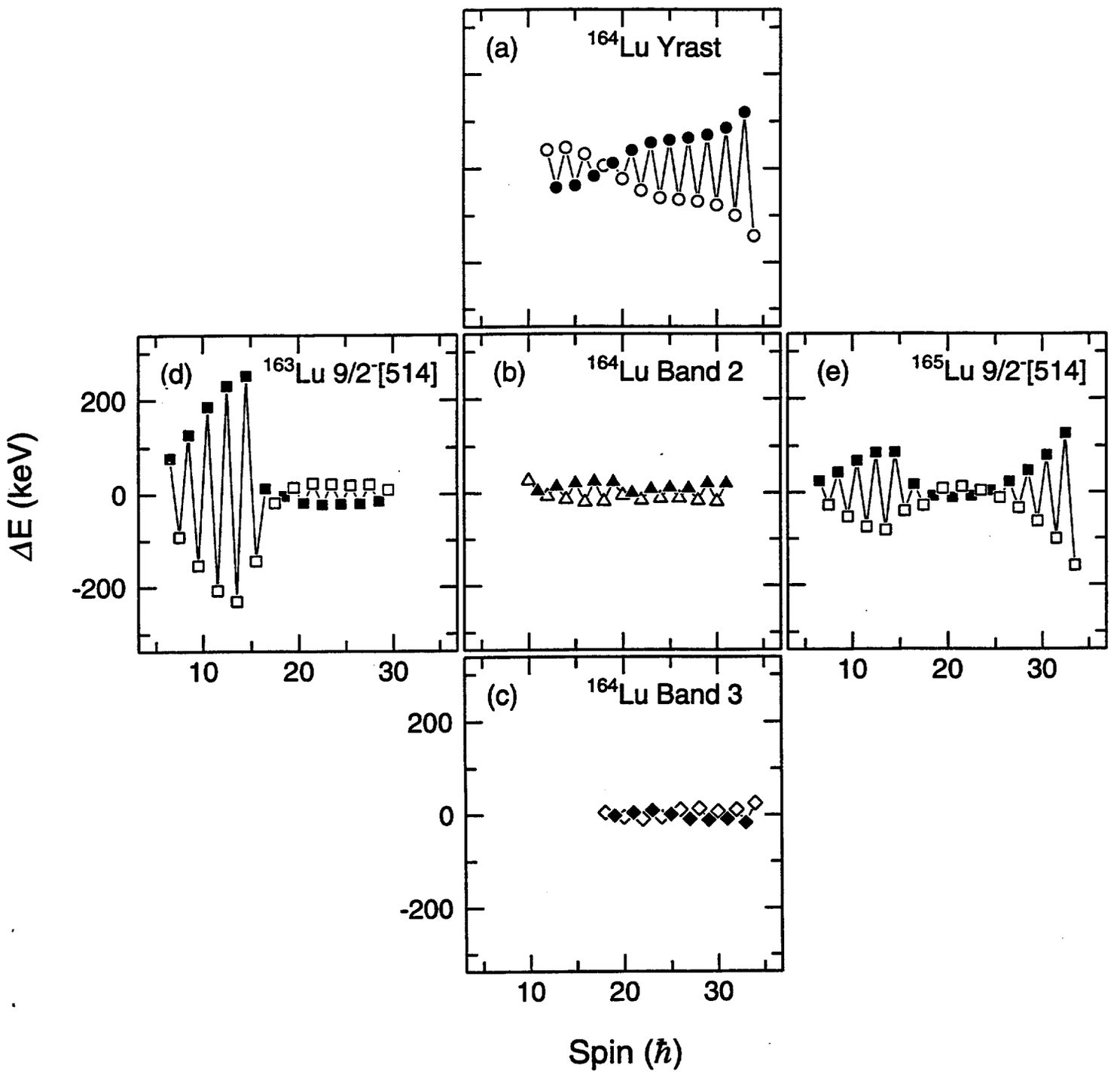

X.-H. Wang, et al, Fig. 13